Doctoral Thesis

The Peptidergic Control Circuit for Neuroendocrine Dynamics in Rats

ラット神経内分泌動態におけるペプチド性制御機構に関する研究

Keita Satoh

2017

Contents

General Introduction

The neuroendocrine system is composed of the interaction between neural and endocrine systems responding to environmental stimuli (Fig. 1). The expression and release of neurohormones are regulated by physiological conditions (Fig. 1). Neurohormones are mainly synthesized as a part of a preprohormone precursor containing the signal peptide and neurohormones (Burbach, 2010). After signal peptide removal in the endoplasmic reticulum, the prohormone is sorted and packaged into vesicles in the Golgi apparatus (Fig. 1). The prohormone in vesicles is then subjected to a post-translational modification by co-packaged processing enzymes during its axonal transport to terminals (Burbach, 2010). The neurohormone is released from axon terminal by exocytosis and involved in physiological function *via* specific receptors of each neurohormone (Burbach, 2010). On the other hand, neurons expressing neurohormones form neural neural network by synaptic connections, and this neural network modulate the neuroendocrine system (Burbach, 2010). To elucidate the peptidergic control circuit of the neuroendocrine system, it is important to develop an excellent model that visualizes molecular dynamics and neural network of neurohormone. In addition, the molecular basis of post-translational processing of neurohormones is remained unclear (Burbach, 2010). Furthermore, it is difficult to analyze the neural network because there are few methods to extensively visualize the neural network composed of ultrastructure including synapses. In this study, it is confirmed the imaging model that visualizes neurohormone *in vivo* molecular dynamics. In addition, application of the special heavy metal stain to three-dimensional (3-D) ultrastructural observation enables to perform an effective 3-D and comprehensive ultrastructure (*connectome*) analysis.

Arginine vasopressin (AVP), one of neurohormones, is produced in neuronal

cell bodies of hypothalamus and released mainly from the axon terminal projected to the posterior pituitary. Released AVP directly modulates peripheral organs *via* the circulation. A transgenic (Tg) rat line which expresses the AVP-enhanced green fluorescent protein (eGFP) fusion gene has been generated (Ueta *et al.*, 2005; Fujio *et al.*, 2006; Shibata *et al.*, 2007; Suzuki *et al.*, 2009b; Maruyama *et al.*, 2010). AVP-eGFP Tg rats provide a unique model for visualizing the molecular dynamics of AVP *in vivo* and for live imaging and/or electrophysiology of identified AVP neurons without any specific histological labeling (Ueta *et al.*, 2005; Fujio *et al.*, 2006; Shibata *et al.*, 2007; Suzuki *et al.*, 2009b; Maruyama *et al.*, 2010). Previous studies have demonstrated that the exposure of AVP-eGFP Tg rats to dehydration induced significantly greater expression of GFP in PVN and SON neurons, mirroring to that of native AVP (Ueta *et al.*, 2005; Fujio *et al.*, 2006). However, there is no evidence whether GFP, an exogenous protein is released into the circulation. Additionally, the *in vivo* molecular dynamics and exocytosis of GFP in response to physiological stimuli may differ from those of native AVP, because the molecular size of GFP is much greater than AVP (approximately 30 times). In Chapter 1, to study *in vivo* molecular dynamics of neurohormone using AVP-eGFP Tg rats, the *in vivo* molecular processing of AVP-eGFP fusion gene was analyzed, and the physiological response of GFP release into the circulation was also verified.

The 3-D analysis of anatomical ultrastructures is important in most fields of biological research. However, it is considerably difficult to perform a 3-D image analysis of exact serial sets of ultrathin sections. Although 3-D reconstruction from ultrathin sections has been generally used to obtain 3-D information, this technique is applicable only for small specimen areas because of the technical and physical

difficulties under the transmission electron microscopy (TEM). Since synapses are a small structure (submicron order) in neurons, they are only able to be analyzed using the TEM. Therefore, the structural analysis of a population of synaptic inputs is difficult to perform methodologically and requires a time-consuming analysis at the ultrastructural level (Hayworth *et al.*, 2014; Henny *et al.*, 2014; Ohno *et al.*, 2015). Because normal TEM has a limitation of specimen thickness which is generally less than a hundred nanometers, the structural information in ultrathin sections is mostly 2-D (Hama & Kosaka, 1981; Sakamoto & Kawata, 2012). It is, therefore, difficult to use this approach for visualization of 3-D structures in biological specimens at either whole cellular and/or organotypic levels. On the other hand, high-voltage electron microscopy (HVEM) has higher penetration power of the electrons due to the increased accelerating voltage (~1,000 kV) and enables us to examine thicker sections of biological specimens (Sakamoto *et al.*, 2010; Oti *et al.*, 2012). Thus, HVEM should be particularly useful to analyze the 3-D ultrastructures of micrometer-sized tissues at the nanometer level (volume electron microscopy) (Hama & Kosaka, 1981; Sakamoto & Kawata, 2012). Important findings have recently demonstrated that spinal itch transmission is independent of pain transmission and relies on gastrin-releasing peptide (GRP)/GRP receptor signaling in the dorsal horn of the spinal cord (Sun & Chen, 2007; Sun *et al.*, 2009), as well as in the trigeminal sensory system in the medulla oblongata (Takanami *et al.*, 2014). These new findings are a major breakthrough in this research field (Sun & Chen, 2007; Sun *et al.*, 2009). At the ultrastructural level, the spinal dorsal horn contains numerous synaptic connections locally that are important in conveying somatosensory inputs from the periphery, although the chemical neuroanatomy of the synapses involved in the itch sensation

remains elusive (Takanami & Sakamoto, 2014). In Chapter 2, using an immune-HVEM tomography with a high-contrast *en bloc* staining method, the chemical 3-D neuroanatomy of the rat spinal dorsal horn was revealed by immunohistochemistry at the ultrastructural level. This new approach also attempts an effective *connectome* analysis and is a novel method of 3-D electron microscopy.

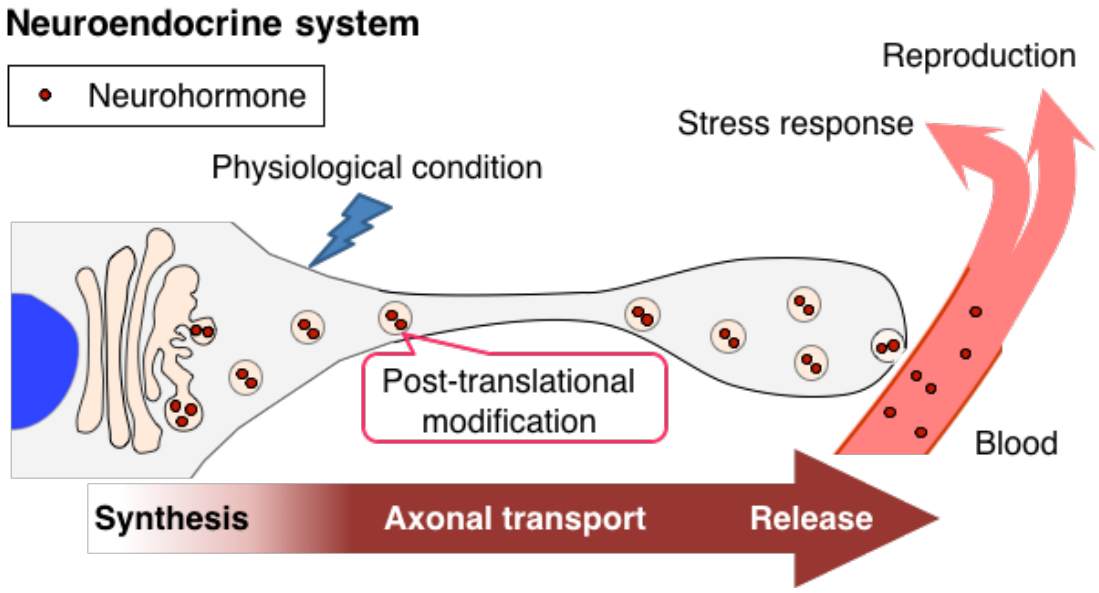

Figure 1.

Schematic drawing of the neuroendocrine system. Peptidergic neuromodulators (neurohormone) are mainly synthesized as a part of a preprohormone precursor containing a signal peptide and the bioactive hormones. After signal peptide removal in the endoplasmic reticulum, the prohormone is sorted and packaged into vesicles in the Golgi apparatus. The prohormones in vesicles are then subjected to a post-translational modification by co-packaged processing enzymes during the axonal transport to terminals.

Chapter 1

In Vivo Imaging Model Visualizing the Molecular Dynamics of Neurohormones

Summary

Arginine vasopressin (AVP) is a neurohypophysial hormone synthesized as a part of a prepropeptide precursor, containing the signal peptide, AVP hormone, AVP-associated neurophysin II and copeptin in the hypothalamic neurosecretory neurons. A transgenic (Tg) rat line expressing the AVP-enhanced green fluorescent protein (eGFP) fusion gene has been generated. To establish the AVP-eGFP Tg rat as a unique model for an analysis of the AVP dynamics *in vivo*, it was first examined the *in vivo* molecular dynamics of the AVP-eGFP fusion gene, and then the release of GFP in response to physiological stimuli. Double immunoelectron microscopy demonstrated that GFP was specifically localized in neurosecretory vesicles of AVP neurons in this Tg rat. The stimulation of the posterior pituitary with high potassium achieve the exocytosis of AVP neurosecretory vesicles containing GFP at the ultrastructural level. Biochemical analyses indicated that the AVP-eGFP fusion gene is subjected to *in vivo* post-translational modifications like the native AVP gene, and is packaged into neurosecretory vesicles as a fusion protein: copeptin$_{1\text{-}14}$-GFP. Moreover, GFP release into the circulating blood appeared to be augmented after osmotic stimulation, like native AVP. Thus, it shows that for the first time the *in vivo* molecular processing of the AVP-eGFP fusion gene and stimulated secretion after osmotic stimulation in rats. Because GFP behaved like native AVP in the hypothalamo-pituitary axis, and was especially released into the circulation in response to a physiological stimulus, the AVP-eGFP Tg rat model appears to be a powerful tool for analyzing neuroendocrine systems at the organismal level.

Introduction

Arginine vasopressin (AVP) is produced mainly by magnocellular neurosecretory cells (MNCs) in the paraventricular (PVN) and supraoptic (SON) nuclei of the hypothalamus. These MNCs primarily project to the pituitary through the median eminence, and AVP is released into the blood circulation from their axon terminals in the neurohypophysis and also into the surrounding neuropil from magnocellular dendrites (Pow & Morris, 1989; Castel *et al.*, 1996; Ludwig *et al.*, 2002). The expression and release of AVP in MNCs are regulated by physiological conditions, including the osmotic balance and blood pressure (Koshimizu *et al.*, 2012). AVP is synthesized as a part of a prepropeptide precursor containing the signal peptide, AVP hormone, AVP-associated neurophysin (NP) II and a glycopeptide copeptin (CP) (see Fig. 1A) (Land *et al.*, 1982; Davies *et al.*, 2003). After signal peptide removal in the endoplasmic reticulum, the propeptide is sorted and packaged into neurosecretory vesicles in the Golgi apparatus (Davies *et al.*, 2003). The AVP propeptide in neurosecretory vesicles is then subjected to a post-translational modification by co-packaged processing enzymes during its axonal transport to terminals in the neurohypophysis (Davies *et al.*, 2003). In the neurohypophysis, the exocytotic release of AVP into blood vessels is induced by Ca^{2+} influx into the axonal terminals by MNC electrical activity evoked by various physiological stimuli (Cazalis *et al.*, 1985). However, the molecular dynamics of the AVP gene expression and the exocytotic activity from terminals and/or dendrites remain unclear *in vivo*.

A transgenic (Tg) rat line which expresses the AVP-enhanced green fluorescent protein (eGFP) fusion gene was generated about ten years ago (Ueta *et al.*,

2005; Fujio *et al.*, 2006; Shibata *et al.*, 2007; Suzuki *et al.*, 2009b; Maruyama *et al.*, 2010) (see Fig. 1B). AVP-eGFP Tg rats provide a unique model for visualizing the molecular dynamics of AVP *in vivo* and for live imaging and/or electrophysiology of identified AVP neurons without any specific histological labeling (Fujihara *et al.*, 2009; Ohbuchi *et al.*, 2009; Suzuki *et al.*, 2009a; Ohbuchi *et al.*, 2010; Todoroki *et al.*, 2010; Iwanaga *et al.*, 2011; Moritoh *et al.*, 2011; Ohkubo *et al.*, 2014). Previous studies have demonstrated that the exposure of AVP-eGFP Tg rats to dehydration induced significantly greater expression of GFP in PVN and SON neurons, mirroring to that of native AVP (Ueta *et al.*, 2005; Fujio *et al.*, 2006). Recently, with fiber-optic probes 'optrodes', a rapid increase in green fluorescence has been reported in the neurohypophysis of AVP-eGFP Tg rats after intravenous administration of hypertonic saline (Yao *et al.*, 2011). The increased fluorescence following an osmotic cue is thought to be due to pH changes following eGFP release (Yao *et al.*, 2011). These results suggest that, using GFP as a reporter, it may be possible to monitor AVP release from the neurohypophysis *in vivo* in real-time in response to a physiological stimulation (Yao *et al.*, 2011). However, the *in vivo* molecular dynamics and exocytosis of GFP in response to physiological stimuli may differ from those of native AVP, because the molecular size of GFP is much greater than AVP (approximately 30 times). In this study, therefore, using AVP-eGFP Tg rats, it is first examination the *in vivo* molecular processing of AVP-eGFP fusion gene, and verified the physiological response of GFP release into the circulation, to establish a unique model for analyses of the AVP dynamics at the organismal level.

Materials and Methods

Animals

AVP-eGFP Tg male and WT male 10- to 14-week-old rats were used in this study. The generation of AVP-eGFP Tg rats has been described previously (Ueta *et al.*, 2005). All pups were screened by PCR analysis of genomic DNA extracted from ear biopsies according to the method described previously (Ueta *et al.*, 2005). Heterozygous AVP-eGFP Tg and WT littermates (for controls) were bred and housed in two rats per cage at 24-26ºC on a 12-hour light, 12-hour dark cycle. All animals used in this study were allowed free access to water and rodent chow unless they were part of the salt-loading experiment. All experimental procedures were performed in strict accordance with guidelines on the use and care of laboratory animals as set out by the Physiological Society of Japan and approved by the Ethics Committee of Animal Care and Experimentation of University of Occupational and Environmental Health, Japan, and have been authorized by the Committee for Animal Research, Okayama University, Japan.

Double immunoelectron microscopy

AVP-eGFP Tg males (n = 4) were deeply anesthetized with ip injections of 50 mg/kg body weight sodium pentobarbital, and transcardially perfused with physiological saline followed by 4% paraformaldehyde and 0.1% glutaraldehyde in 0.1 M phosphate buffer (PB; pH 7.4). The posterior pituitaries were quickly removed and immersed in 4% paraformaldehyde in 0.1M PB for 3 hours at room temperature, then

dehydrated through increasing concentrations of methanol, embedded in LR Gold resin (Electron Microscopy Sciences, PA, USA), and polymerized under UV lamps at –20ºC for 24 hours. Ultrathin sections (70 nm in thickness) were collected on nickel grids coated with a collodion film, rinsed with phosphate buffered saline (PBS; pH 7.4) several times, then incubated with 1% normal goat serum and 2% BSA in 50 mM tris(hydroxymethyl)-aminomethane-buffered saline (TBS; pH 7.6) for 30 minutes to block non-specific binding. The sections were then incubated with a 1:20 dilution of a rabbit mAb against GFP (Cell Signaling Technology Japan, Tokyo, Japan) and 1:150 dilution of a mouse mAb against AVP-associated NP II (PS41) (Castel *et al.*, 1986) for 2 hours at 30ºC or 1:200 dilution of a mouse mAb against oxytocin-associated NP I (PS60) (Castel *et al.*, 1986) for 1 hour at room temperature. These PS41 and PS60 antibodies have previously shown to be specific for AVP and oxytocin neurons, respectively (Castel *et al.*, 1986; Wang *et al.*, 1995; Sakamoto *et al.*, 2007). After incubation with the primary antibodies, the sections were washed with PBS, then incubated with a 1:50 dilution of a goat antibody against rabbit IgG conjugated to 5 nm gold particles (BBI Solutions, Cardiff, UK) and a goat antibody against mouse IgG conjugated to 15 nm gold particles (BBI Solutions) for 1 hour at room temperature. Finally, the sections were contrasted with uranyl acetate and lead citrate and viewed using an H-7650 electron microscope (Hitachi, Tokyo, Japan) operated at 80 kV.

GFP-immunoprecipitation and Western blotting

AVP-eGFP Tg (n = 7) and WT (n = 7) males were killed by decapitation under deep pentobarbital anesthesia (see above). Pituitaries were quickly removed, placed on ice, and the posterior pituitaries were carefully dissected out under a dissecting

microscope (Olympus, Tokyo, Japan), snap-frozen immediately in liquid nitrogen, and used for GFP-IP. The GFP-IPs were performed using 1/20 posterior pituitary from each Tg male with a GFP-Trap-A kit (ChromoTek GmbH, Planegg-Martinsried, Germany; using a camel Fab fragment directed against the GFP whole molecule) according to the manufacturer's protocol. The preparations (1/20 posterior pituitary protein/lane before IP was subjected in this study) from Tg and WT rats were boiled in 10 μl sample buffer containing 62.5 mM trishydroxymethyl-aminomethane-HCl (Tris-HCl; pH. 6.8), 2% SDS, 25% glycerol, 10% 2-mercaptoethanol, and a small amount of bromophenol blue. These samples were run on a 4-20% SDS-PAGE and electroblotted onto a polyvinylidene difluoride membrane (Bio-Rad Laboratories, Hercules, CA, USA) from the gel by a semidry blotting apparatus (Bio-Rad Laboratories). The blotted membranes were blocked with 3% BSA and 0.05% Tween 20 in TBS (TBST) for 30 minutes at room temperature and incubated for 2 hours at 30ºC with a 1:1,000 dilution of rabbit mAb against GFP (Cell Signaling Technology Japan), or for 1 hour at room temperature in Can Get Signal Solution 1 (TOYOBO, Tokyo, Japan) with a 1:5,000 dilution of a rabbit polyclonal antibody against rat CP-fragment: $CP_{7\text{-}14}$ (ATQLDGPA) that was generated to label N-terminal region of CP (by us in this study). The blotted membranes were washed three times with TBST and incubated with horseradish peroxidase-conjugated goat polyclonal antibody against rabbit IgG (Bio-Rad Laboratories) 1:100,000 dilution in Can Get Signal Solution 2 (TOYOBO) for 1 hour at room temperature. After washing for three times with TBST, blots were visualized by Immun-Star WesternC Chemiluminescence Kit (Bio-Rad Laboratories). Control procedures consisted of: 1) preabsorbing the working dilution (1:5,000) of the primary antiserum with a saturating concentration of the antigen (20 μg/ml; ATQLDGPA); and

2) substituting pre-immune rabbit serum for the primary antiserum in a dilution of 1:5,000 (data not shown). The blots were also incubated with these control sera according to the same procedure as the antiserum.

After stripping the primary antibodies with 62.5 mM Tris-HCl buffer (pH 6.7) containing 2% SDS and 100 mM 2-mercaptoethanol for 1 hour at room temperature and washing with TBST, blots were then subjected to second immunoreactions as dual immunolabeling for CP or NP II (PS41: 1:1,000 dilution) and GFP to determine the molecular weight of the immunopositive bands as described above.

Exocytosis of GFP in the neurohypophysis revealed by a double immunoelectron microscopy *ex vivo*

To study exocytosis of the GFP-fusion protein, neurohypophyses of Tg males were stimulated *ex vivo* with 56 mM potassium according to the method described previously with slight modifications (Pow & Morris, 1989; Castel *et al.*, 1996). In brief, AVP-eGFP Tg males (n = 4) were killed by decapitation under a deep pentobarbital anesthesia; their posterior pituitaries were quickly removed onto ice and cut into small pieces (~2 mm in size) with a sterilized razor. The tissue pieces were then incubated with artificial cerebrospinal fluid (aCSF) pre-gassed with 95% O_2/5% CO_2 for 15 minutes at 37ºC, then incubated with aCSF containing a high level (56 mM) of potassium and 0.2% tannic acid for 15 minutes at 37ºC. After the high-potassium stimulation *ex vivo*, the pituitary pieces were immersed in 4% paraformaldehyde and 0.1% glutaraldehyde in 0.1 M PB for 3 hours at room temperature, washed with 0.1 M PB, then processed for the ultrastructural analysis of exocytoses by double immunoelectron microscopy for GFP and NP II as described above.

Biochemical analyses for GFP release from the neurohypophysis and its physiological response *in vivo*

A salt-loading model according to the previous studies (Fujio *et al.*, 2006; Katoh *et al.*, 2011) was employed to examine whether GFP is released into the circulating blood and the plasma level of GFP-fusion protein is increased. AVP-eGFP Tg (n = 6) and WT males (n = 6) were given 2% salt solution instead of water to drink for 5 days. After salt-loading, these salt-loaded and control Tg males (n = 6 each) were killed by decapitation under deep pentobarbital anesthesia. Trunk blood was collected and the plasma separated by centrifugation. The posterior pituitaries were also quickly removed onto ice, snap frozen in liquid nitrogen, and used for GFP extraction (1/20 posterior pituitary protein/lane was used as the positive control). The GFP fusion protein was extracted from the plasma of each group (1 ml plasma/lane before IP was loaded onto each lane) with a GFP-Trap-A Kit (using camel antibodies), followed by Western blotting for GFP using the rabbit mAbs for GFP as described above.

For quantitative analysis, it was determined the OD of each immunoreactive band derived from salt-loaded and control Tg males by use of Image Lab Software (Bio-Rad Laboratories). The OD in the salt-loaded Tg males was calculated as the ratio to the OD of control Tg males, and data are expressed as the mean ± standard error of the mean. The data were analyzed using an unpaired Student's t-test. Statistical significance was set at $P < 0.05$.

Results

In vivo subcellular localization of GFP in AVP neurons by immunoelectron microscopy

To examine whether the fusion gene encoded AVP preproprotein containing GFP is translated and packaged within the neurosecretory vesicles with the AVP, it was performed to analyze the subcellular localization of GFP in the posterior pituitary of AVP-eGFP Tg rats by a double immunoelectron microscopy. In this experiment, GFP-immunoreactivity (ir) was labeled with 5 nm-diameter colloidal gold particles, and AVP-associated NP II-ir or oxytocin-associated NP I-ir was labeled with 15 nm-diameter colloidal gold particles (Fig. 2). As shown in Figure 2A, NP II-ir and GFP-ir were both detected only in the terminals of neurosecretory axons, and co-associated on the neurosecretory vesicle structures in the same terminal (Fig. 2, A and B). In contrast, no GFP-ir was detected in a juxtaposed NP II-unlabeled terminal area, a putative oxytocin terminal (Fig. 2C). Similarly, double labeling for NP I and GFP (Fig. 2, D-F) showed that GFP-ir was not observed in the NP I-positive terminal, but was present in the NP I-negative terminal (Fig. 2, D-F).

In vivo post-translational modification of AVP-eGFP fusion gene revealed by immunoprecipitation (IP) and Western blotting

To examine the post-translational modifications of the AVP-eGFP fusion gene, we next performed a Western analysis for GFP and NP II on the same membrane. Figure 3A shows that an intense GFP-ir band was detected in the posterior pituitaries of Tg

males, but was not detected in those of wild-type (WT) males. Judging from its electrophoretic mobility, the molecular mass of this GFP-ir protein band was 28 kDa (Fig. 3A). After GFP-immunoprecipitation (IP), the major GFP-ir band was only detected at the same level of 28 kDa (Fig. 3A). No specific GFP-ir band was detected at the other molecular weight levels (Fig. 3A). After stripping the GFP antibodies, blots were subjected to the second immunoreaction for NP II antibodies. This showed a single NP II-ir band at 10 kDa in the neurohypophyses of both WT and Tg males, but no 10 kDa ir band in the GFP-IP proteins from Tg males (Fig. 3B). Subsequently, a Western analysis was performed using anti-$CP_{7\text{-}14}$ antiserum, because of the translation product in the Tg rats was expected $CP_{1\text{-}14}$ (see Fig. 1). We performed immunoreactions first for $CP_{7\text{-}14}$ and next for GFP on the same membrane (Fig. 4). As shown in Figure 4A (the right panel), an intense $CP_{7\text{-}14}$-ir band at 28 kDa was observed in the posterior pituitary of Tg males. After GFP-IP, a single $CP_{7\text{-}14}$-ir band was detected also at 28 kDa in the blots (Fig. 4A, the right panel). Because the molecular mass of whole CP is approximately 4 kDa, 28 kDa is the expected total molecular mass of the $CP_{1\text{-}14}$ (AREQSNATQLDGPA: ~1 kDa) and GFP (~27 kDa) fusion protein (Fig. 1B). However, no $CP_{7\text{-}14}$-ir band was detected at 38 kDa (Fig. 4A) the expected for a size of a tri-fusion protein consisting of $CP_{1\text{-}14}$ (~ 1 kDa), GFP (~27 kDa) and NP II (~10 kDa) (Fig. 1B). After stripping $CP_{7\text{-}14}$ antibodies, the blots were re-incubated with a GFP mAb. Although some higher molecular weight bands were visible at about 32~36 kDa for $CP_{7\text{-}14}$ (Fig. 4A), an intense and single GFP-ir band at 28 kDa was observed in each blot (Fig. 4B), possibly corresponding to the $CP_{7\text{-}14}$-ir band on the same membrane (Fig. 4A) when these panels are compared. However, no 28 kDa $CP_{7\text{-}14}$-ir band was observed in the neurohypophysis of WT males (Fig. 4A, the left panel). In addition, no $CP_{7\text{-}14}$-ir

band was detected at ~4 kDa expected for the size of native CP both in Tg and WT males (Fig. 4A). Because preabsorbed antiserum also detected these higher molecular weight bands, they are possibly non-specific (Fig. 4A, the middle panel).

Release of GFP into the peripheral blood and its induction by salt-loading

To examine the release of GFP from AVP terminals by exocytosis at the ultrastructural level, high potassium stimulation was employed to induce exocytosis in the neurohypophysis. As shown in Figure 5A and 5B, many double (NP II and GFP)-positive neurosecretory vesicles formed close appositions with the plasma membrane of AVP axons (*arrows*). Some NP II-ir neurosecretory vesicles with higher electron density (due to binding of the tannic acid) were located in the extracellular space near AVP neuron terminals of Tg males (Fig. 5, C and D, *arrows*). In addition, GFP-ir 5-nm gold particles were also observed on the exocytotic (Fig. 5B, *arrowheads*) and secreted (Fig. 5D, *arrowheads*) neurosecretory vesicles with higher electron density.

Finally, it was examined whether GFP is released into the circulating blood, and further examined the effect of salt-loading on the induction of GFP release as well as that of native AVP. Western analysis using anti-GFP was first performed to determine the presence of GFP in plasma after the GFP-IP extraction. As a positive control, an intense GFP-ir band at 28 kDa was also observed in the homogenized posterior pituitaries from Tg rats (Fig. 6A, *Pituitary*). In the plasma extracts from non-salt-loaded Tg rats, a feeble GFP-ir band was also observed at the similar molecular size (Fig. 6A, *the middle panel of Plasma*). After salt-loading a much stronger GFP-ir band was observed in the plasma extracts from Tg rats, mirroring the release of AVP (Fig. 6A, *the right panel of Plasma*). In contrast, no GFP-ir band was observed in the plasma extracts

of salt-loaded WT rats (Fig. 6A, *the left panel of Plasma*), nor of naïve WT rats (data not shown). Quantitative analysis of GFP-ir bands in the plasma extracts showed that the bands from salt-loaded Tg males were of significantly higher optical density (OD) than those from control Tg males ($n = 6$ in each group) (Fig. 6B) ($^*P < 0.05$).

Discussion

Three-dimensional (3-D) analysis of synaptic connections (*synaptome*) is

The aim of this present study was to examine *in vivo* molecular processing of the AVP-eGFP fusion gene in rats, and to establish a useful model for analyses of the AVP dynamics *in vivo*. In this Tg rat line, the GFP gene is inserted into the middle of the CP gene (see Fig. 1B), and expected to be translated as a part of AVP preproprotein (Ueta *et al.*, 2005). We first examined the subcellular localization of GFP in AVP-eGFP Tg rats. Double immunoelectron microscopy demonstrated that GFP-ir was detected in AVP-associated NP II-ir neurosecretory vesicles but not in oxytocin-associated NP I-ir neurosecretory vesicles in the posterior pituitary of AVP-eGFP Tg rats. This shows that GFP is specifically localized in neurosecretory vesicles of AVP neurons in this Tg rats. Therefore, in AVP-eGFP Tg rats, an AVP preproprotein linked to GFP appears to be synthesized in the cell bodies, packaged into neurosecretory vesicles, and transported to axon terminals of AVP neurons in the posterior pituitary *in vivo* in the same way as native AVP. The normal AVP proprotein is processed to its constituent parts in neurosecretory vesicles (Davies *et al.*, 2003). Western analysis demonstrated that the pituitary of Tg rats contains a 28 kDa-ir band with both $CP_{7\text{-}14}$ and GFP antibodies. No NP II-ir band could be detected after GFP-IP, suggesting that the GFP fusion proteins do not contain any NP II protein. These results demonstrate that the AVP-eGFP fusion gene is subjected to the same post-translational modifications as the native AVP gene to produce a fusion protein: $CP_{1\text{-}14}$-GFP *in vivo*. On the other hand, in this GFP-Western analysis, some lower molecular weight bands (at 10 kDa and about 15-20 kDa) could

not be immuno-precipitated from the pituitary of Tg rats, (see Fig. 3A, IP+). We suggest that a part of the GFP is cleaved into two pieces (*e.g.* 10 and 18 kDa), both of which are detected by the rabbit monoclonal antibody used for the Western blotting. Alternatively, the bands could represent small proteins other than GFP recognized by the antibody used for the Western blotting, but not by the antibody used for IP (camel Fab fragment). The much stronger 10 kDa NP II-ir band in Tg rats than in WT rats (see Fig. 3B) also suggests that in Tg rats more NP II is stored in AVP neurons, leading to the conclusion that in Tg rats more AVP-eGFP fusion gene is expressed than native AVP gene in WT rats, although the level of circulating AVP is almost normal in AVP-eGFP Tg rats as reported previously (Ueta *et al.*, 2005). Notwithstanding this discrepancy, the present and previous studies demonstrated *in vivo* molecular processing of the AVP-eGFP fusion gene, suggesting that bioactive AVP has also been released into the circulation from the AVP precursor prepropeptide in AVP-eGFP Tg rats.

High potassium stimulation of the posterior pituitary of AVP-eGFP Tg rats showed that the fusion protein is also released by exocytosis in the same way as native AVP, NP II and CP. After the high potassium stimulation, many neurosecretory vesicles formed close appositions with the plasma membrane of AVP axons and several showed a higher electron density indicating docking for exocytosis (Buma *et al.*, 1984; Castel *et al.*, 1996), because previous studies have shown that tannic acid can gain access to exocytotic neurosecretory vesicles through the fusion pore, causing a higher electron density (Buma *et al.*, 1984; Morris & Pow, 1988; Castel *et al.*, 1996). We also observed several NP II-ir neurosecretory vesicle cores with a higher electron density located in the extracellular space near AVP neuron terminals (see Fig. 5, C and D). These appeared to have been secreted from the adjacent AVP terminal by exocytosis. Furthermore, some

gold particles indicating the presence of GFP and NP II released by exocytosis were also detected in the boundary area of the extracellular space.

Finally, using IP and Western combined analyses, a GFP-ir band was detected in the plasma of AVP-eGFP Tg rats, suggesting that the released GFP circulates like native AVP. Substantial evidence has demonstrated that the expression level and release of AVP are both significantly increased by osmotic stimulation (Sherman *et al.*, 1986; Kawasaki *et al.*, 2005; Ueta *et al.*, 2005). Recently, it has also been reported that GFP signals in the hypothalamus and posterior pituitary of AVP-eGFP Tg rats are considerably amplified by salt-loading (Fujio *et al.*, 2006). It is demonstrated here that the GFP-ir band in plasma extracts was amplified in extracts from salt-loaded Tg rats. Thus, not only the expression of AVP-eGFP fusion gene (Ueta *et al.*, 2005; Fujio *et al.*, 2006), but also the release of the GFP fusion protein appears to be augmented in response to physiological stimulation. Taken together these results show that, in AVP-eGFP Tg rats, the *in vivo* dynamics of GFP, including its post-translational modifications, packing into neurosecretory vesicles, release into the blood, and response to an important physiological stimulus, mimic those of native AVP. Therefore, the AVP-eGFP Tg rat appears to be an excellent animal model for a number of physio- and/or pathological applications, because a real-time GFP imaging could probably mimic *in vivo* AVP secretion after various physiological or pharmacological stimulations. However, additional studies are required to draw a firm conclusion – currently it is attempting to take sequential samples of the jugular blood, and see if it is possible to detect a change in the plasma GFP of rats subject either to an osmotic or stress stimulus from the fluorescence. Methodological developments are still needed to detect the GFP from a small amount of the plasma sample.

CP, a 39-aminoacid glycopeptide, is the C-terminal part of the AVP precursor prepropeptide. Activation of the AVP system stimulates CP secretion into the circulation in equimolar amounts to AVP. Thus, CP concentration directly reflects AVP secretion and can be used as a surrogate biomarker because of its stability *in vivo* (Bhandari *et al.*, 2009; Blanchard *et al.*, 2013; Wuttke *et al.*, 2013; Bolignano *et al.*, 2014). Little is known about CP functions *in vivo* (Morgenthaler *et al.*, 2006; Balanescu *et al.*, 2011; Kolonko *et al.*, 2014). Because post-translational modification of the AVP-eGFP fusion gene product results in the formation of a fusion protein: copeptin$_{1\text{-}14}$-GFP *in vivo*, AVP-eGFP Tg rats will also make it possible to examine the *in vivo* dynamics of CP by analyzing GFP signals. The plasma concentration of CP fluctuates with plasma osmotic pressure and correlates with that of AVP in humans (Balanescu *et al.*, 2011). Moreover, the plasma concentration of CP appears to be a strong and reliable predictor of mortality in patients with chronic and/or acute heart failure (Bolignano *et al.*, 2014). A higher CP concentration is also associated with kidney function decline, suggesting that CP may be a new marker to predict kidney outcome in autosomal dominant polycystic kidney disease (Boertien *et al.*, 2012). Thus, analyzing the dynamics of CP in AVP-eGFP Tg rats may offer new avenues for potential therapeutic approaches to refractory heart failures or kidney diseases. Interestingly, recent clinical studies in healthy adults also showed 1.2~1.8-fold higher baseline CP level in men than women (Szinnai *et al.*, 2007; Bhandari *et al.*, 2009; Meijer *et al.*, 2010). Furthermore, it has recently been reported that male-dominant production of AVP is a phenomenon already present in newborn infants, leading to higher plasma AVP or CP levels in boys compared to girls (Burckhardt *et al.*, 2014). In human neonates, vaginal delivery is associated with significantly elevated CP level in the umbilical cord blood compared to delivery by

Cesarean section (Schlapbach *et al.*, 2011). Taken together, these results may provide a new insight into the sexual disparity of AVP or CP and its potential implication in postnatal adaptation, especially in response to birth stress, including mode of delivery, perinatal acidosis and asphyxia *etc*. (Burckhardt *et al.*, 2014). However, the significance of the sexual difference in the AVP or CP systems remains unknown. Since only a fragment (possibly $CP_{1\text{-}14}$) of CP is expressed in these Tg rat as part of the fusion protein with GFP, it is not clear if CP would be functional in these Tg rats *in vivo*. In fact, some of the exaggerated responses of this Tg animal might be related to this mutation (Suzuki *et al.*, 2009a). Nevertheless, future studies using AVP-eGFP Tg rats may allow elucidation of this aspect of CP physiology.

This is the first demonstration of an excellent model for *in vivo* analyzing the molecular dynamics of the secretory proteins fused with fluorescent protein. Parvocellular PVN AVP neurons have many terminals within the hypothalamus and also in extrahypothalamic areas, *e.g.*, bed nucleus of the stria terminalis, hippocampus, medulla oblongata and spinal cord, where they appear to play a key role in social behaviors, sexual motivation, pair bonding, and maternal responses to stress (for reviews, see Refs. (Meyer-Lindenberg *et al.*, 2011; Rood & De Vries, 2011; Albers, 2014)). In some of these areas, AVP expression is sexually dimorphic (Rood & De Vries, 2011; Rood *et al.*, 2013; Otero-Garcia *et al.*, 2014). It will be interesting to determine if the GFP is an equally robust reporter in these areas. Substantial evidence further demonstrates that AVP is released by exocytosis fusion not only from neurohypophysial axon terminals of MNCs but also from their dendrites and cell bodies, suggesting neural transmission by the relatively unexplored mechanism of '*dendritic secretion*' (Pow & Morris, 1989; Castel *et al.*, 1996; Ludwig *et al.*, 2002). However, the physiological roles

of and controls on the novel neural transmission mechanism, '*dendritic secretion*' by which AVP (and oxytocin) are released by an exocytosis not only from the axonal terminals but also from the dendrites and cell bodies of MNCs (Pow & Morris, 1989; Ludwig, 1998; Wotjak *et al.*, 1998; Ludwig *et al.*, 2002; Tobin *et al.*, 2012) remain relatively unexplored. Imaging of GFP signals in AVP-eGFP Tg rats should allow investigation of the *in vivo* release of dendritic peptides into the hypothalamus surrounding MNCs. Two-photon laser scanning microscopy is an exciting new fluorescence nanoscopy technique, with lower phototoxicity and higher penetration depth (~1 mm) deeper than the conventional confocal microscopy (Denk & Svoboda, 1997). It has been used to demonstrate insulin secretion from intact mouse pancreatic islets (Takahashi *et al.*, 2002) and fusion pore dynamics in a variety of peripheral endocrine tissues at nanometer resolution (Takahashi *et al.*, 2002; Kishimoto *et al.*, 2006). Total internal reflection fluorescence (TIRF) microscopy (Axelrod, 1981) has also been used to analyze tethering, docking, priming, and fusion of a single dense-core vesicle with associated protein-targeted fluorescent protein variants to reveal molecular mechanisms of exocytosis *in vitro* (Tsuboi & Fukuda, 2005; 2006a; b; Tsuboi *et al.*, 2007; Sato *et al.*, 2012). Thus, the establishment of the AVP-eGFP Tg rat model demonstrated in this paper could be used with fluorescence nanoscopy and imaging analyses to investigate the dynamics of neurohormone secretion in neurosecretory cells at the organismal level.

In conclusion, here it is showed for the first time the *in vivo* molecular processing of AVP-eGFP fusion gene and the stimulated secretion of its products after osmotic stimulation in rats. Because the GFP behaved like native AVP in the hypothalamo-pituitary axis, and was also released into the circulation in response to a

physiological stimulus, the AVP-eGFP Tg rat model appears to be a powerful tool for analyzing neuroendocrine systems at the organismal level.

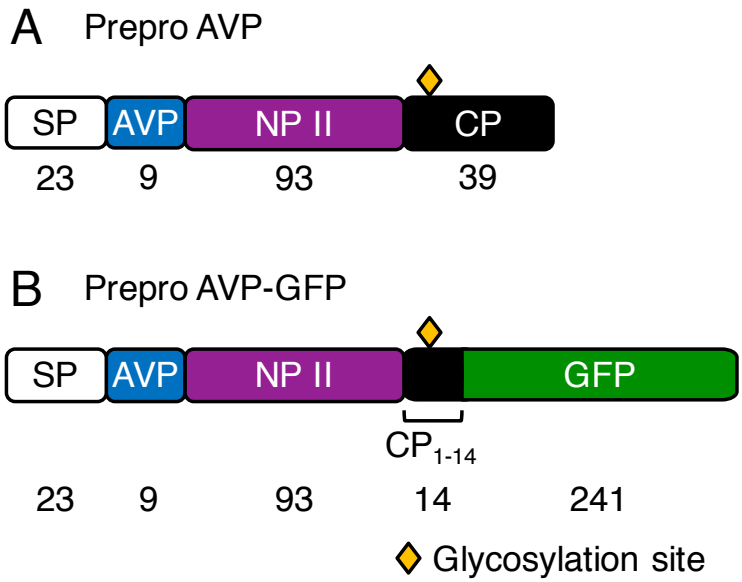

Figure 1.

Schematic structures of arginine vasopressin (AVP) preproprotein and the AVP-green fluorescent protein (GFP) fused preproprotein. AVP preproprotein (A) and AVP-GFP fusion preproprotein (B) are consisting of the signal peptide (SP), AVP hormone, AVP-associated neurophysin (NP) II and the glycoprotein copeptin (CP), where the glycan is represented by a *diamond*. The translation as a $CP_{1\text{-}14}$ is expected in this transgene, and the sixth asparagine of CP is expected to be a glycosylation site. The *numbers* denote the amino acids present in each region.

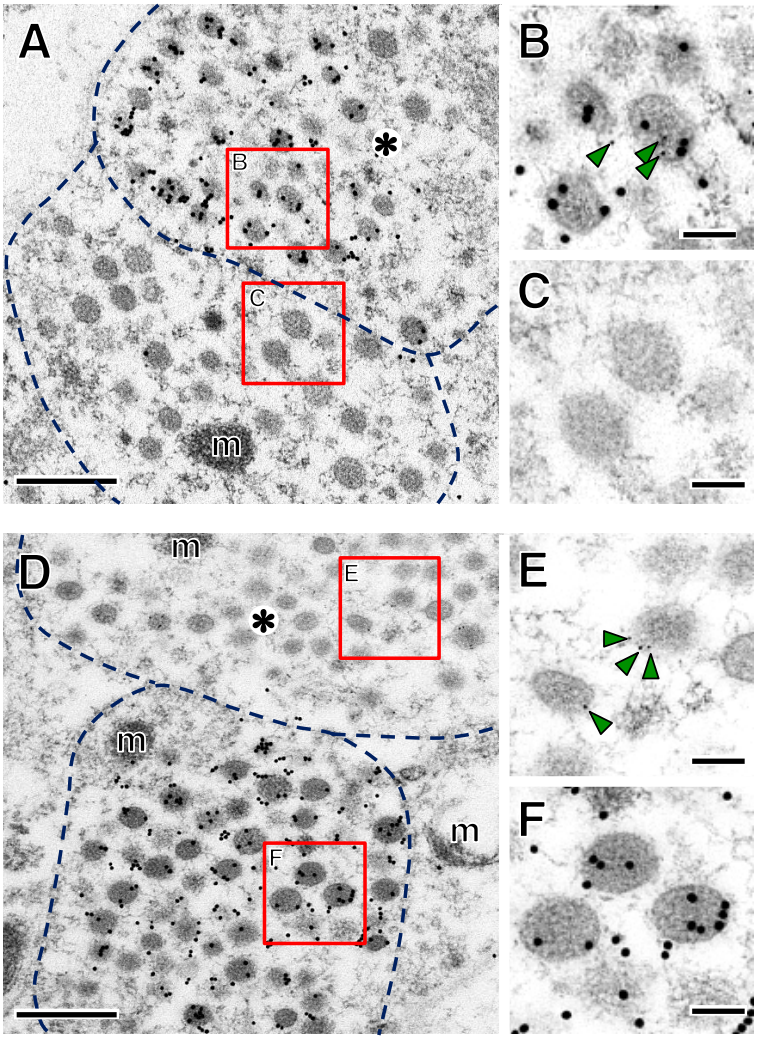

Figure 2.

Double immunoelectron microscopy of the AVP-eGFP transgenic (Tg) rat neurohypophysis. GFP and NP I/II antibodies labeled with 5 nm and 15 nm gold particles, respectively. Each *blocked area* in (A and D) are enlarged in (B and C) and (E and F), respectively. AVP terminals (*asterisk* in A and D) include GFP-positive (*arrowheads* in B and E) neurosecretory vesicles. Otherwise, juxtaposed oxytocin terminals were both negative for GFP (C and F). *Dashed lines* indicate putative boundary of terminals. Immunocytochemical studies were repeated independently four times by using different males and gave similar results. *m*, mitochondrion. *Scale bars*, 500 nm (A and D); 100 nm (B, C, E and F).

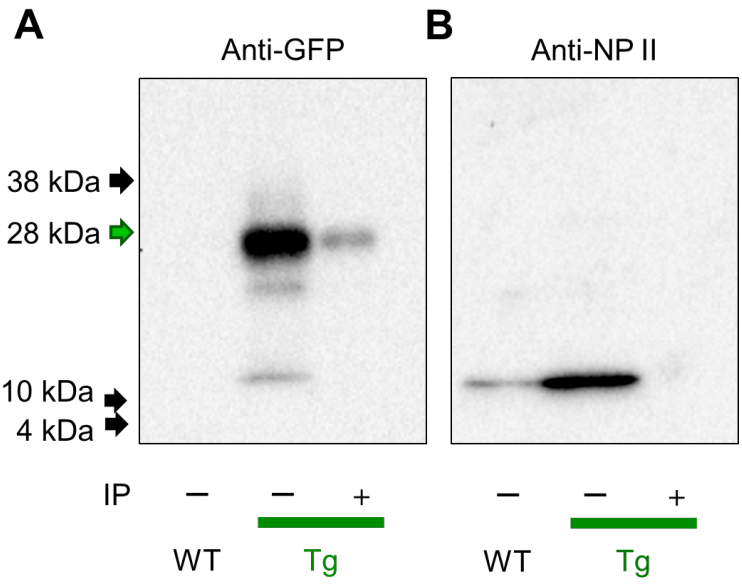

Figure 3.

The expression of *GFP* in the posterior pituitary of AVP-eGFP Tg rats. In A, *GFP*-positive band was observed at 28 kDa in the *Tg* posterior pituitaries, but not in *WT* (A). After *GFP*-immunoprecipitation (*IP*), the *GFP*-positive band was only detected at the same level of 28 kDa (A). After the second-incubation with *NP II* antibodies, *NP II*-positive bands at 10 kDa were detected in the posterior pituitaries of both *WT* and *Tg* rats (B). *GFP-IP* also showed that *NP II*-like protein band was not detected in the *GFP-IP* blots of *Tg* rats (B). Western analyses were repeated independently three times by using different samples and gave similar results. The *minus* (-) and *plus* (+) signs indicate with and without *IP*, respectively.

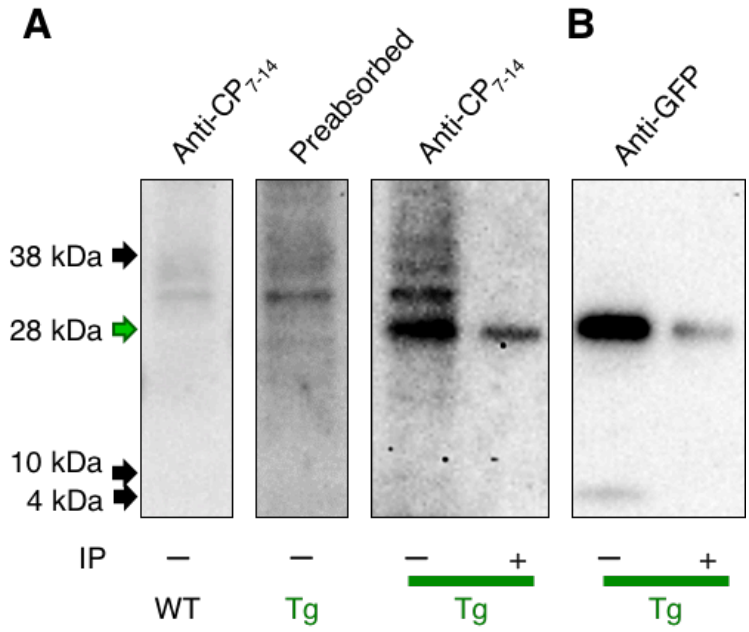

Figure 4.

The expression of *CP1-14* and *GFP* fusion protein in the posterior pituitary of AVP-eGFP Tg rats. (A) An intense *CP7-14*-positive band was observed at 28 kDa in Tg rats (the left panel). On the other hand, *Preabsorbed* working solution of the primary *CP7-14* antiserum with a saturating concentration of the antigen peptide (20 μg/ml; ATQLDGPA) before use completely eliminates the 28 kDa-protein band (the middle panel). As expected, no *CP7-14*-positive band was detected at 28 kDa in *WT* rats (the right panel). In addition, no *CP7-14*-positive band was detected at ~4 kDa expected for the size of native CP both in *Tg* and *WT* rats. After *GFP-IP*, the *CP7-14*-positive band was only detected at the same level of 28 kDa (B). The second-incubation with *GFP* antibodies demonstrated that the *CP7-14*-positive proteins appeared to exist as *CP1-14* and *GFP* fusion proteins (B). Western analyses were repeated independently three times by using different samples and gave similar results.

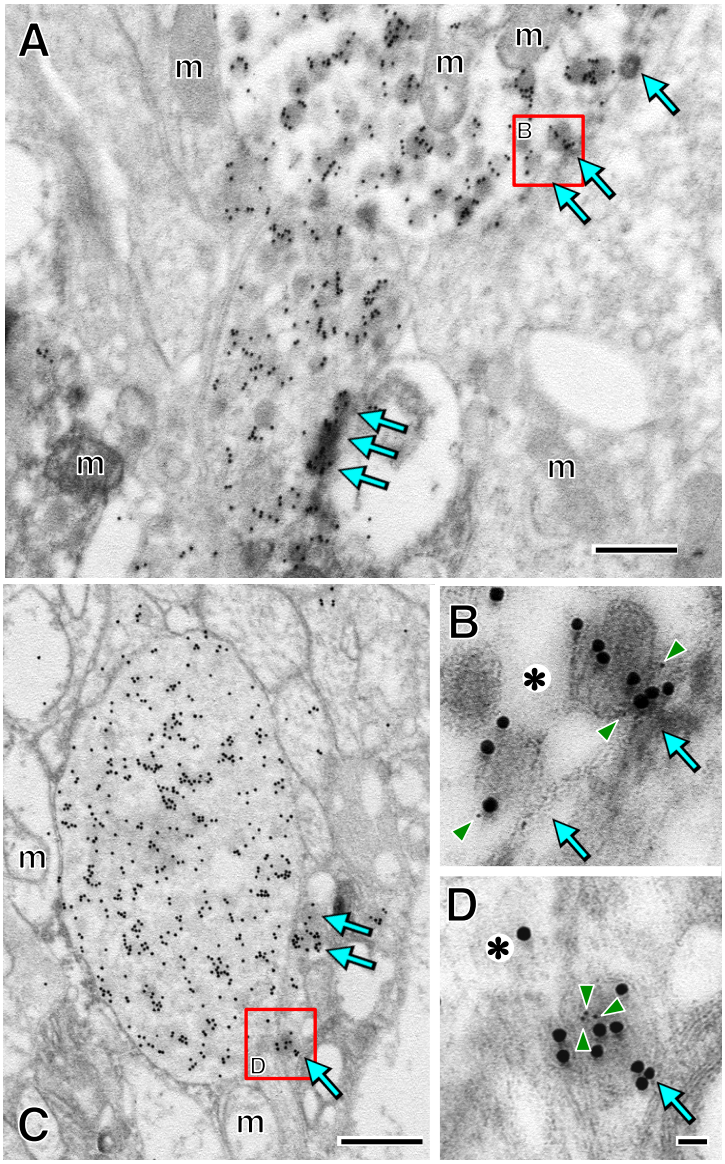

Figure 5.

A post-embedding ultrastructual analysis of GFP exocytosis induced by the high potassium stimulation in the posterior pituitary of Tg rats. (A and B) Axon terminals containing numerous neurosecretory vesicles, many of which lie close to the plasmalemma, a position appropriate to render them readily available for release. Double immunoelectron microscopy for GFP (labeled with 5 nm gold particles; *arrowheads* in B and D) and NP II (labeled with 15 nm gold particles) revealed that some double positive neurosecretory vesicles appeared to be undergoing exocytosis (*arrows* in A and B). A GFP exocytotic figure is clearly visible (*arrows* in C and D). *Asterisks* in B and D indicate inside of AVP terminals. *Ex vivo* exocytosis studies were repeated independently four times by using different Tg males and gave similar results. *m*, mitochondrion. *Scale bars,* 500 nm (A and C); 100 nm (B and D).

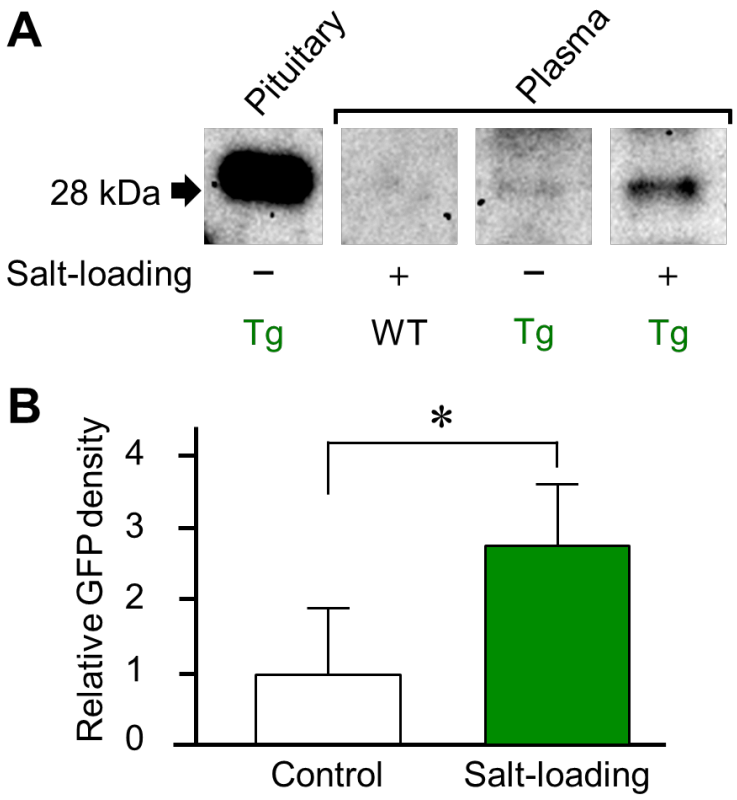

Figure 6.

GFP release into the circulating blood and its response to salt-loading. (A) Western analysis for GFP showed that a feeble GFP-positive band was detected in the GFP-IP extracts from *Tg* plasma, but not in *WT*. Neurohypophyses of *Tg* rats was loaded as a positive control. An enhanced GFP-positive band was observed in the plasma extracts of salt-loaded *Tg* rats. (B) Quantitative analysis of GFP-positive bands in the extracts also revealed that salt-loaded *Tg* males displayed a significantly higher optical density than control *Tg* males ($n = 6$ in each group). Western analyses were repeated independently three times by using different samples and gave similar results. *$P < 0.05$.

Chapter 2

The Effective Three-dimensional *Synaptome* Analysis by the High-voltage Electron Microscopy Tomography

Summary

Transmission electron microscopy (TEM) is used for three-dimensional (3-D) analysis of synaptic connections in neuroscience research. However, 3-D reconstruction of the synapses using serial ultrathin sections is a powerful but tedious approach requiring advanced technical skills. High-voltage electron microscopy (HVEM) allows examination of thicker sections of biological specimens due to the increased penetration of the more accelerated electrons, which is useful to analyze the 3-D structure of biological specimens. However, it is still difficult to visualize the neural networks and synaptic connections in 3-D using HVEM because of insufficient and non uniform heavy metal staining in the membranous structures in semi-thin sections. Here, it present the successful chemical 3-D neuroanatomy of the rat spinal dorsal horn at the ultrastructural level as a first step for effective *synaptome* analysis by applying a high-contrast *en bloc* staining method to immune-HVEM tomography. New approach made it possible to examine many itch-mediating synaptic connections and neural networks in the spinal cord simultaneously using HVEM tomography. This novel 3-D electron microscopy is very useful for the analysis of synaptic structure and the chemical neuroanatomy at the 3-D ultrastructural level.

Introduction

Three-dimensional (3-D) analysis of synaptic connections (*synaptome*) is important in neuroscience research. Because synapses are a small structure (submicron order) in neurons, they are only able to be analyzed using either transmission electron microscopy (TEM) or scanning electron microscopy (SEM), and thus, the 3-D organization of synaptic connections revealed by serial ultrathin sections requires a time-consuming analysis in both TEM and SEM (Hayworth *et al.*, 2014; Henny *et al.*, 2014; Inami *et al.*, 2015). Although a combination of immunohistochemistry (IHC) and confocal laser scanning microscopy allows imaging and quantification of the 3-D organization of biological specimens, the ultrastructural morphology of the cells, including synaptic connections, remains obscure due to the insufficient spatial resolution of light microscopy (Okabe, 2013). The poor visualization of the structures remains a problem even if fluorescent visualization methods are used, and unlabeled (non-fluorescing) domains cannot be observed (Belichenko & Dahlstrom, 1995; Miyawaki, 2003; Nishi & Kawata, 2006). Because normal TEM has a limitation of specimen thickness which is generally less than a hundred nanometers, the structural information in ultrathin sections is mostly 2-D (Hama & Kosaka, 1981; Sakamoto & Kawata, 2012). It is, therefore, difficult to use this approach for visualization of 3-D structures in biological specimens at either the cellular and organotypic levels. On the other hand, high-voltage electron microscopy (HVEM) has higher penetration power of the electrons due to the increased accelerating voltage (~1,000 kV) and enables us to examine thicker sections of biological specimens (Sakamoto *et al.*, 2010; Oti *et al.*,

2012). Thus, HVEM should be particularly useful to analyze the 3-D ultrastructures of micrometer-sized tissues at the nanometer level [volume electron microscopy (EM)] (Hama & Kosaka, 1981; Sakamoto & Kawata, 2012).

Important findings have recently demonstrated that spinal itch transmission is independent of pain transmission and relies on gastrin-releasing peptide (GRP)/GRP receptor signaling in the dorsal horn (DH) of the spinal cord (Sun & Chen, 2007; Sun *et al.*, 2009), as well as in the trigeminal sensory system in the medulla oblongata (Takanami *et al.*, 2014). These new findings are a major breakthrough in the studies on the molecular basis of itch (Sun & Chen, 2007; Sun *et al.*, 2009). At the ultrastructural level, the spinal DH contains numerous synaptic connections locally that are important in conveying somatosensory inputs from the periphery, although the chemical neuroanatomy of the synapses involved in the itch sensation remains elusive (Takanami *et al.*, 2014). In this study, using an immune-HVEM tomography with a high-contrast *en bloc* staining method, it is successfully described the chemical 3-D neuroanatomy of the rat spinal DH revealed by IHC at the ultrastructural level. This new approach also attempts an effective *synaptome* analysis and is a novel method of 3-D EM.

Materials and Methods

Animals

Adult male Wistar rats were obtained from the Charles River Laboratories Japan (Yokohama, Japan). All experimental procedures have been authorized by the Committees for Animal Research, Okayama University and Kyoto Prefectural University of Medicine, Japan.

GRP IHC and EM

Male rats (n = 9) were overdosed with sodium pentobarbital and perfusion fixed with 4% paraformaldehyde, 0.1% glutaraldehyde, and 0.3% tannic acid in 0.1 M phosphate buffer. Cervical spinal cords were immediately removed and immersed in 4% paraformaldehyde in 0.1 M phosphate buffer for 3 h. Spinal sections (C3–C6 level; 30 μm in thickness) were prepared with a LinearSlicer® (Dosaka EM, Kyoto, Japan). The free-floating sections were thoroughly washed with phosphate buffered saline (PBS) and preincubated in PBS containing 0.05 % Triton X-100, 1 % normal goat serum, and 1 % BSA for 30 min at room temperature to block nonspecific reactions. Sections were then incubated with the primary rabbit antiserum against rat $GRP_{20\text{-}29}$ (1:1,000) (AssayPro, St. Charles, MO, USA) overnight at room temperature with gentle agitation. The GRP antiserum used in this study have previously shown to be specific for rat GRP in the spinal cord (Takanami *et al.*, 2014). Immunoreactive (ir) products were detected with a streptavidin-biotin kit (Nichirei, Tokyo, Japan), followed by diaminobenzidine development, as described previously (Takanami *et al.*, 2014). Some immunostained

sections were first viewed using a light microscope for reference after dehydration and clearing. The other stained sections were then subjected to special *en bloc* staining according to the protocol of the National Center for Microscopy and Imaging Research (NCMIR), University of California, San Diego, CA, USA with slight modifications (Deerinck *et al.*, 2010). The NCMIR method is widely used for serial block-face SEM (SBF-SEM), which was designed to enhance signal for backscatter electron imaging of epoxy-embedded mammalian tissue at low accelerating voltages (Deerinck *et al.*, 2010). This sample preparation method for effective heavy metal staining was applied to *synaptome* analysis by HVEM tomography. Briefly, after being washed with 0.15 M cacodylate buffer, the sections were post-fixed for 1 h in 2% aqueous osmium tetroxide/1.5% potassium ferrocyanide in 0.15 M cacodylate buffer, for 20 min in a thiocarbohydrazide solution, and then for 30 min in a 2% osmium tetroxide solution. Sections were placed in 1% uranyl acetate overnight at 4°C and then in a lead aspartate solution in a 60°C oven for 30 min. The sections were dehydrated and flat embedded in epoxy resin (Quetol-812; Nisshin EM, Tokyo, Japan). For reference, some sections were embedded without the above *en bloc* staining and post-fixed with 1% osmium tetroxide for 2 hours instead as conventional EM-IHC. Ultrathin sections (70 nm in thickness) containing the GRP-ir fibers in the DH were prepared and collected on mesh grids coated with a collodion film. First, the preparations were viewed and imaged with an H-7650 electron microscope (Hitachi, Tokyo Japan) without any additional heavy metal staining at an accelerating voltage of 80 kV. After the TEM observations, the same sections were stained with both uranyl acetate and lead citrate. These heavy metal-stained sections were then viewed and imaged again using the same TEM condition, and the images were compared with the former non-stained sections.

Subsequently, semi-thin sections (1-2 μm in thickness) containing the GRP-ir fibers in the DH were then prepared and collected on mesh grids coated with a collodion film. Each grid-mounted semi-thin section was first selected using a light microscope (Olympus; BH-2, Tokyo, Japan). Selected grids or sections were observed using an HVEM (Hitachi H-1250M; National Institute for Physiological Sciences, Okazaki, Japan) at an accelerating voltage of 1,000 kV.

Tomography

The specimen was tilted from -60.0° to +60.0° and imaged at 1-dgree steps (121 images per view; 0.0, ±1.0 ~ ±60.0). The images were digitized and 3-D models were constructed using IMOD software (Kremer *et al.*, 1996; Pettersen *et al.*, 2004). Individual subcellular and organelle structures were observed by UCSF Chimera and manually segmented using the AMIRA software package (FEI Visualization Science Group, Burlington, MA, USA) (Pettersen *et al.*, 2004). This software package was also used to generate the 3-D image figures.

Results

Using conventional light microscopy, IHC analysis of the EM preparations first showed that GRP-ir fibers were densely stained in the superficial layers of the cervical spinal DH (laminae I-II) in a similar way as reported previously (Sun & Chen, 2007; Fleming *et al.*, 2012; Takanami *et al.*, 2014) (n = 3) (*arrowheads* in Fig. 1A, B). After pre-embedding using the GRP IHC method, the stained sections were then flat-embedded in epoxy resin and observed by conventional light microscopy again (Fig. 1C). Numerous GRP-ir terminals were also visible in the spinal DH (laminae I-II) (n = 3) (*arrowheads* in Fig. 1C), whereas the IHC-stained and resin-embedded sections with NCMIR method did not identify any GRP-ir due to the heavy *en bloc* staining (n = 3) (Fig. 1D). *Arrowheads* in Figure 1D indicate the region of laminae I-II, possibly including regions of numerous GRP-ir. The ultrathin sections (60 nm), including regions of laminae I-II (*arrowheads* in Fig. 1C) without any additional heavy metal staining, showed the presynaptic terminals containing the GRP-ir (*asterisk*) and the synaptic connection (*double arrows*) with low contrast using conventional TEM (Fig. 1E). On the other hand, when these sections were contrasted with the heavy metal staining, many GRP-ir vesicles were then clearly visualized in the presynaptic terminal (*asterisk*), and the electron-dense postsynaptic density (PSD) (*double arrows*) was also visible (Fig. 1E'). Subsequently, the ultrathin sections, including regions of laminae I-II (*arrowheads* in Fig. 1D) without any additional heavy metal staining, were examined using a conventional TEM with the NCMIR method *en bloc* staining (Fig. 1F). The fine membranous structures, including the electron-dense GRP-ir presynaptic terminal

(*asterisk*) and surrounding structures, were observed (Fig. 1F).

Next, using HVEM, it was observed the NCMIR-treated semi-thin sections (1-2 μm in thickness) of laminae I-II (*arrowheads* in Fig. 1D) without any additional heavy metal staining (Fig. 2). Figure 3 shows a representative HVEM image. Numerous synaptic contacts were clearly visualized, and the GRP-ir products were observed as fine fuzzy materials widely distributed in the terminal-like structures of the superficial layers of the cervical spinal cord (laminae I-II) (Fig. 3A). Using a semi-thin section, a lower magnification HVEM image (Fig. 3A) was similar to some extent in quality to the images acquired by conventional TEM using serial ultrathin sections (Fig. 1F). Subsequently, using a higher magnification image, stereopaired HVEM images obtained by tilting the specimen stage ±8° clearly showed that multiple synaptic contacts of GRP neurons were easily identified in a single semi-thin section (Fig. 3B, B'). GRP-ir presynaptic terminals contained several mitochondria and formed synapses with postsynaptic neurons with the PSD (*double arrows* in Fig. 3B). A total of 121 images per view were obtained by tilting the specimen from -60.0° to +60.0°, continuously. The 3-D reconstruction was performed from these 121 serial-tilted images (Fig. 4, Supplementary Movie 1 in Ref (Satoh *et al.*, 2015). GRP-ir presynaptic terminals formed a varicose-like structure, and each varicose-like structure tended to not only contain some mitochondria but also form a synapse (Fig. 4A, B). These terminals connected with postsynaptic neurons with PSD, which was observed as a gray zone in proximity to membranous structures using conventional TEM (*double arrows* in Fig. 4B, C, Supplementary Movies 2, 3 in (Satoh *et al.*, 2015). The 3-D reconstruction from sequential HVEM images using a combination of IHC with the NCMIR method demonstrated a useful and effective *synaptome* methodology, showing a 3-D

visualization of the itch-mediating neural network in the spinal DH at the ultrastructural level (for more details, see Supplementary Movies 1-3 in Ref (Satoh *et al.*, 2015). Since a set of serial semi-thin sections prepared by the pre-embedding method was observed in this study, an intense immunoreaction might frequently be observed in approximately ~10 μm depth from the tissue surface. These 3-D reconstruction analyses were performed for 6 views, in total, from 4 different semi-sections, which were randomly selected from 3 different male rats, and similar results were obtained in all of these samples in this study.

Discussion

HVEM is a powerful method to analyze the 3-D ultrastructures from intense signals, such as heavy osmification (*i.e.*, myelinated fibers or the other conjugated structures having a lipid-rich component), Golgi staining, and immunoreactions (diaminobenzidine reaction products), whereas it was previously difficult to visualize the neural network and synapse structure because of the insufficient contrast of each fine membranous structure in semi-thin sections (Hama & Kosaka, 1981; Hashimoto *et al.*, 2015). In this paper, immune-HVEM tomography applied the NCMIR method, which was originally developed for an enhancement of the membranous contrast for backscattered block-face imaging using SEM, successfully visualized the 3-D structure of the itch-mediating neural networks at the ultrastructural synapse level. This *synaptome* analysis by HVEM effectively detected numerous itch-mediating synaptic connections in the spinal DH in semi-thin sections. Consequently, by observing a single semi-thin section, it was more easily found multiple GRP-ir synaptic connections in the laminae I-II of the spinal cord than that observed with a conventional serial TEM technique (Takanami *et al.*, 2014). Although these results might not be able to detect all of the synapses, a larger number of GRP-ir synapses than expected were visualized in the spinal DH. This methodology could thus successfully allow analysis in a precise volume EM. In addition, GRP-ir presynaptic axonal terminals tended to form a varicose-like structure, which has multiple synapses in the spinal DH. Since it is well accepted that most pre-synaptic axonal terminals contain mitochondria, each GRP-ir varicose-like structure might contain a mitochondrion in this study. It is therefore

suggested that the identified synapses might be functional. Taken together, these results indicated that spinal itch transmission is mediated through the multiple synapses containing GRP in the rat spinal DH.

TEM observations are excellent for synapse analysis because of the high resolution, whereas the information obtained from conventional TEM is mostly 2-D due to the ultrathin property of the tissue (Hama & Kosaka, 1981; Hashimoto *et al.*, 2015). TEM also requires highly skilled investigators to make hundreds or even thousands of serial ultrathin sections for 3-D analysis (Henny *et al.*, 2014). Moreover, it is time consuming to acquire images consecutively for a target observation area even if a series of serial sections can be produced (Henny *et al.*, 2014). In contrast, HVEM can easily analyze a lot of tissue volume and obtain useful information by a single observation on thicker tissue preparations (maximum ~5 μm in thickness), and the 3-D reconstruction analyses of a few some semi-thin sections using HVEM appear to be equivalent to the data obtained from hundreds of serial ultrathin sections using conventional TEM (Sakamoto *et al.*, 2010; Oti *et al.*, 2012). However, a major difficulty in HVEM tomography to obtaining a fine membranous resolution was previously unresolved even though HVEM has the high penetration power of electrons (Hama & Kosaka, 1981; Hashimoto *et al.*, 2015). In this study, application of the NCMIR method to immune-HVEM tomography enables us to perform an effective *synaptome* analysis with a higher contrast of the membranous structures, similarly to TEM resolution. Thus, using this methodology, 3-D information on a large number of synapses can be efficiently obtained from a single semi-thin section.

There have been recent advances of imaging techniques for 3-D reconstruction, including the superfine morphological structures observed with

focused ion beam-SEM (FIB-SEM) and SBF-SEM (Denk & Horstmann, 2004; Briggman & Denk, 2006; Knott *et al.*, 2008; Namba *et al.*, 2015). These new devices can produce consecutive ultrathin sections automatically with either milling with a gallium ion beam or slicing with a diamond knife, and permit the 3-D reconstruction of a large tissue volume, *i.e.*, the thickness of several hundred micrometers, with visualization of the 3-D subcellular structures or organelles at a fine nanometer scale resolution (Denk & Horstmann, 2004; Briggman & Denk, 2006; Knott *et al.*, 2008; Namba *et al.*, 2015). Novel "HVEM tomography" might, at least in part, be superior to such ultra-microtome or beam-milling techniques in terms of quick and repeated examinations. Compared with these 3-D SEM methods, "HVEM tomography" has the following characteristics and advantages: 1) quick observation of a large area, 2) less thermal denaturation, and also 3) no tissue destruction. While the SEM-image acquisition time is limited by the scanning speed, "HVEM tomography" (semi-thin sections) only needs the time required to collect a whole tilt series of the specimen. This is a relatively short acquisition time. The spatial resolution of these 3-D SEMs is possibly superior to "HVEM tomography". However, this approach is less laborious and does not require advanced skills compared with recently developed 3-D SEMs because the ultrastructural information is all in a semi-thin section. In addition, these 3-D SEM analyses destroy the surface of the sample while acquiring the image. As a result, when using these 3-D SEM analyses, it is not possible to observe the same sample repeatedly. Furthermore, the disrupted pieces may sometimes affect the next image acquisition by contaminating the newly-cleaved block surface. Conversely, "HVEM tomography" is not destructive, and it is possible to analyze the same sample repeatedly without any additional interference. Although FIB- and SBF-SEMs

principally have no limitation for acquisition of volume information, “HVEM tomography” might be able to obtain 3-D information on structures deep in the tissue by analyzing a set of serial semi-thin sections.

An electrically automatic tape-collecting ultra-microtome (ATUM) apparatus has also been developed in recent years (Schalek *et al.*, 2011b; Hayworth *et al.*, 2014). One advantage of the ATUM is that it is capable of making ultra-thin sections continuously. A critical advantage is that pre- and post-embedding immune-EMs are possible with the ATUM/SEM. However, despite the convenient automatic collection, there are still possible problems with the failure of collecting sections, some wrinkles or contamination in both the sections and tapes, and failure of heavy metal staining. Since section orientations collected by the ATUM are not always uniform, taking the time to adjust the fine alignment and subsequent normalization of the series of images are still required. Therefore, HVEM tomography may also have some advantages, compared with the ATUM, and be more effective in the volume EM analysis with less failure after identification of an observation area by light microscopy. Thus, HVEM methodology is more useful and effective because it correlates well between light and electron microscopes. On the other hand, a major advantage of these 3-D SEMs is that it is possible to acquire an exact series of the high contrast images, which is the same as a set of TEM images obtained from a number of serial ultra-thin sections. Thus, there are many advantages in both the new 3-D imaging techniques and HVEM tomography, and each technique has specific advantages.

In summary, this new methodology using HVEM tomography combined with IHC is useful for the 3-D analysis of both synaptic connections and chemical

neuroanatomy at the ultrastructural level, and this is potentially a new research approach/alternative for many laboratories. Because the immune-EM (including dual labeling) is one of the established methodologies in neuroscience research, the methodology can be widely and easily applied in multiple ways at either the cellular and organotypic levels.

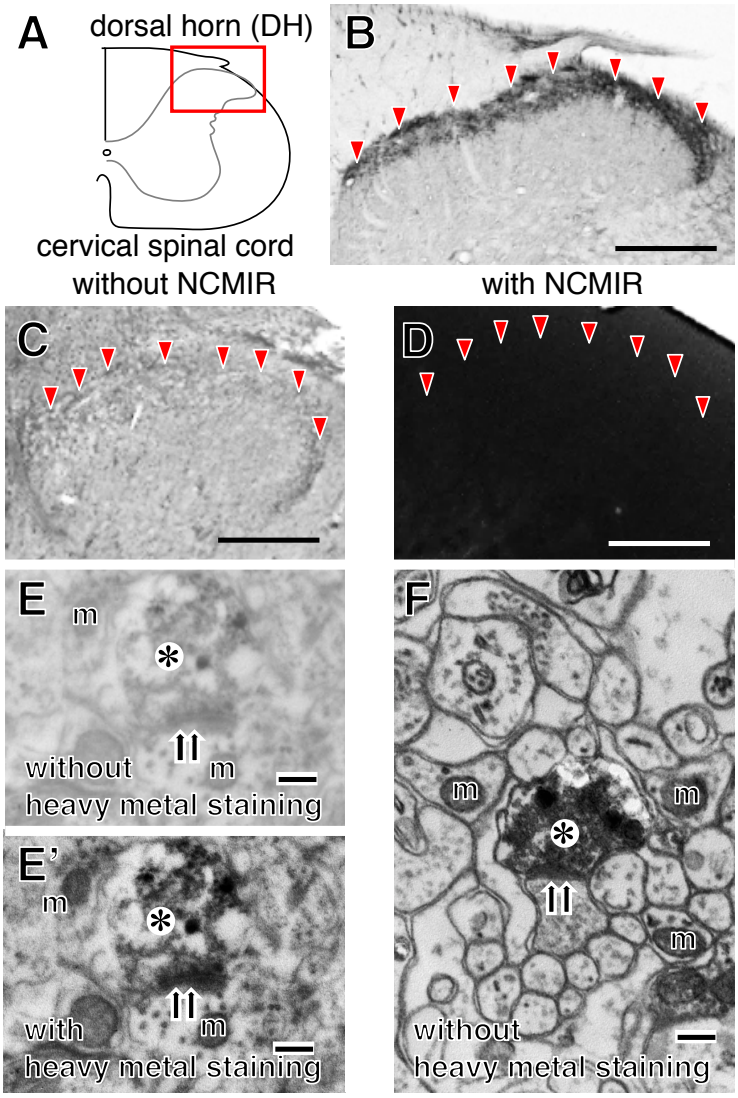

Figure 1.

Comparison of several methodologies for heavy metal staining. (A) The schematic drawing indicates the anatomy of the DH of the cervical spinal cord. (B) Light microscopy reveals that GRP-positive fibers are dense in the superficial layers in the spinal DH. Appearance of flat-embedded spinal sections after GRP-immunostaining (C) and after GRP-immunostaining with the NCMIR method (D). *Arrowheads* indicate possible regions containing numerous GRP-positive terminals (B–D). (E) A low contrast image is shown without any additional heavy metal staining. (E') After the heavy metal staining, the higher contrast membranous structures, including the presynaptic terminal (*asterisk*) and postsynaptic density (*double arrows*), are clearly visible. (F) The fine membranous structures include the electron-dense GRP-positive presynaptic terminal (*asterisk*), synaptic connection (*double arrows*), and surrounding structures without any additional heavy metal staining after the NCMIR method *en bloc*. These (E), (E') and (F) images are obtained from ultrathin sections. *m*, mitochondrion. *Scale bars*, 200 μm (B–D); 200 nm (E, E', and F).

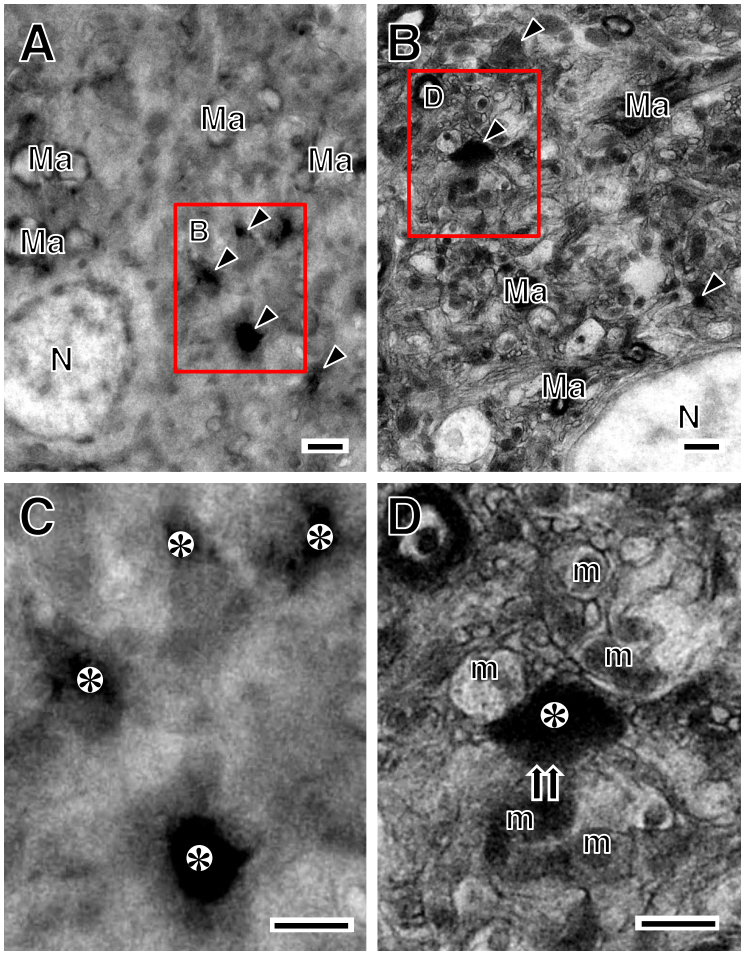

Figure 2.

HVEM images are obtained from semi-thin sections, which are contrasted with the heavy metal staining (A) or the NCMIR method (B). *Arrowheads* in (A) and (B) indicate possible GRP-positive terminals. The *boxed areas* in (A) and (B) are enlarged in (C) and (D), respectively. (C) The enlarged area shows that GRP-positive terminals (*asterisks*) are contrasted, but other membranous structures are unclear. (D) In contrast, the fine membranous structures include the electron-dense GRP-positive presynaptic terminal (*asterisk*), synaptic connection (*double arrows*), and surrounding structures without any additional heavy metal staining after the NCMIR method *en bloc*. *Ma*: myelinated axon; *m*: mitochondrion; *N*: nucleus. *Scale bars*, 1 μm.

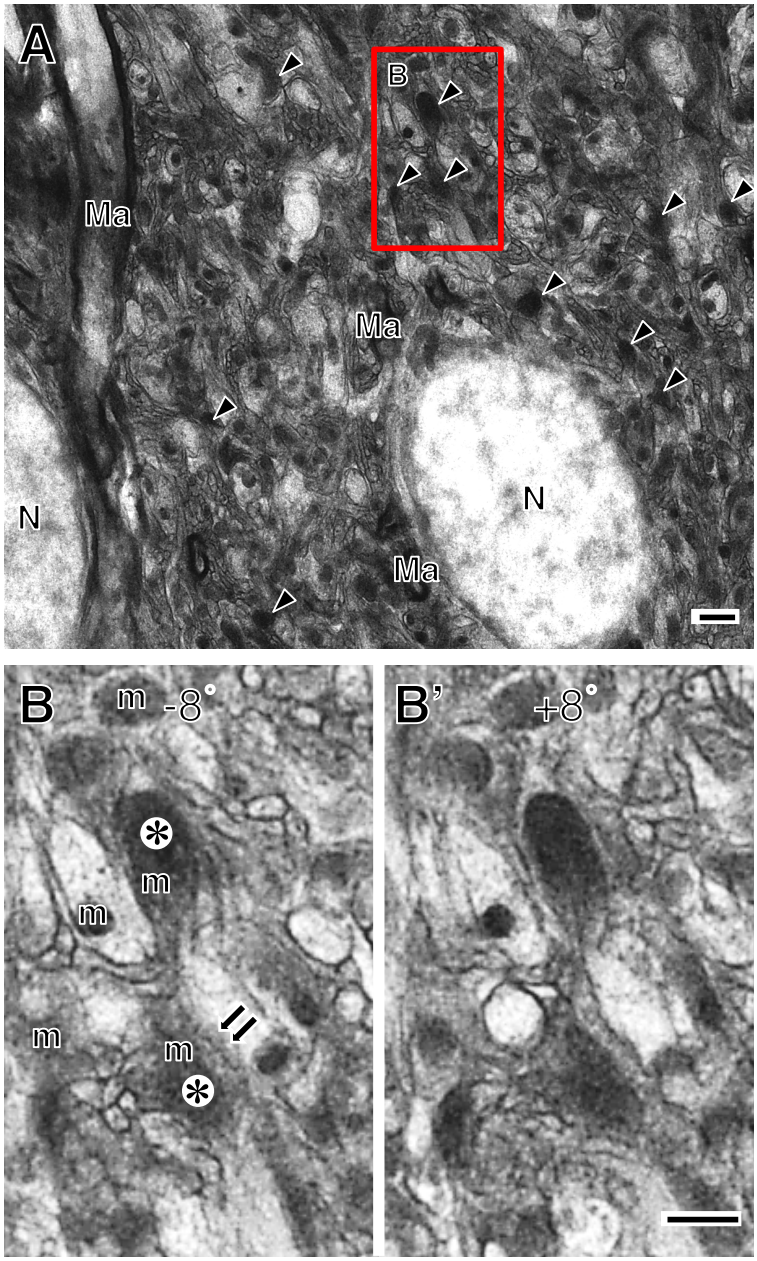

Figure 3.

Representative HVEM images prepared by the NCMIR method. (A) *Arrowheads* indicate possible GRP-positive terminals (for more details, see Supplementary Movie 1 in Ref (Satoh *et al.*, 2015). The boxed area in (A) is enlarged in (B). (B) Stereopaired HVEM images obtained by tilting the specimen stage -8° (B) and +8° (B') show respectively that 3-D GRP-positive terminals (*asterisks*) formed a synaptic contact (*double arrows*) with a dendrite. *Ma*: myelinated axon; *m*: mitochondrion; *N*: nucleus. *Scale bars*, 1 μm (A), 500 nm (B).

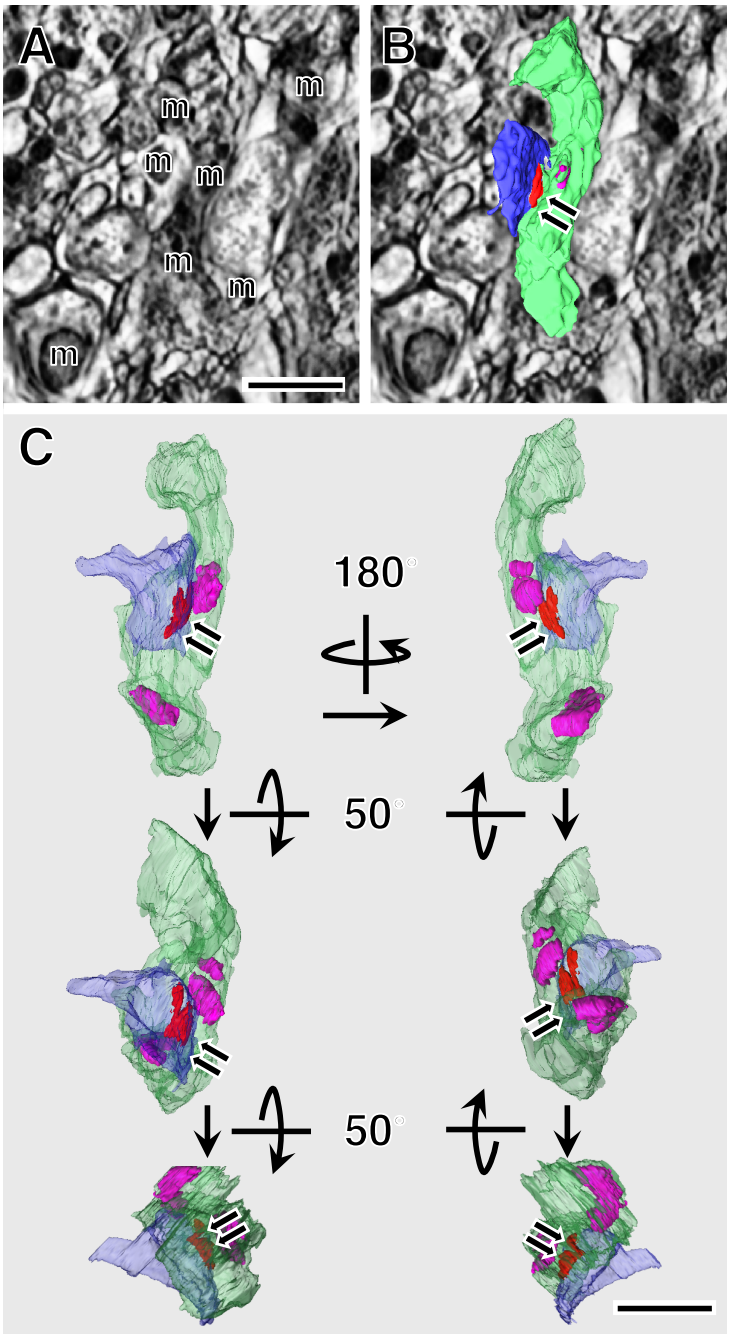

Figure 4.

Three-dimensional analysis for GRP-positive terminals by HVEM tomography. (A) A z-axis slice of the 3-D tomographic reconstruction is shown. (B) GRP-positive terminal (green), postsynaptic dendrite (blue), postsynaptic density (red; indicated by *double arrows*), and mitochondria (magenta) are pseudo-colored, respectively (for more details, see Supplementary Movie 2 in Ref (Satoh *et al.*, 2015). (C) 3-D image figures show representative rotating views (for more details, see Supplementary Movie 3 in Ref (Satoh *et al.*, 2015)). *m*, mitochondrion. *Scale bars*, 1 μm.

General Discussion

Peptidergic neuromodulator (neurohormone) is involved in various physiological functions such as blood pressure control, stress response, and reproduction by the neuroendocrine system (Burbach, 2010). To elucidate the peptidergic control circuit for the neuroendocrine system, it is important to develop an excellent model that visualizes molecular dynamics and neural network of neurohormones. In this study, it was confirmed the imaging model that visualizes neurohormones *in vivo* molecular dynamics. In addition, application of the special heavy metal stain to three-dimensional (3-D) ultrastructural observation was attempted to perform an effective 3-D and comprehensive ultrastructure (*connectome*) analysis. Two neurohormones are focused on in this study: one is arginine vasopressin (AVP) and the other is gastrin-releasing peptide (GRP).

The pleiotropic neurohormone AVP is synthesized in specific neurons principally located in the hypothalamus. AVP is involved in the homeostatic responses numerous life-threatening conditions, for example, the promotion of water conservation during periods of dehydration (Birnbaumer *et al.*, 1992a; Birnbaumer *et al.*, 1992b; Lolait *et al.*, 1992), and the activation of the hypothalamo-pituitary adrenal axis by emotional stress (Viero *et al.*, 2010). A transgenic (Tg) rat line which expresses the AVP-enhanced green fluorescent protein (eGFP) fusion gene has been generated (Ueta *et al.*, 2005; Fujio *et al.*, 2006; Shibata *et al.*, 2007; Suzuki *et al.*, 2009b; Maruyama *et al.*, 2010). In Chapter 1, it has been demonstrated that the AVP-eGFP Tg rat appears to be an excellent animal model for a number of physio- and/or pathological applications, because a real-time GFP imaging could probably mimic *in vivo* AVP secretion after various physiological or pharmacological stimulations. This is the first demonstration of an excellent model for *in vivo* analyzing the molecular dynamics of the fluorescent

protein which expressed as a precursor of secretory protein. It is suggested that the fluorescent protein expressed as part of other neurohormone precursor would be indicate similar molecular dynamics to a native neurohormones. Parvocellular PVN AVP neurons project the hypothalamus and also in extrahypothalamic areas, *e.g.*, bed nucleus of the stria terminalis, hippocampus, medulla oblongata and spinal cord, where they appear to play a key role in social behaviors, sexual motivation, pair bonding, and maternal responses to stress (for reviews, see Refs. (Meyer-Lindenberg *et al.*, 2011; Rood & De Vries, 2011; Albers, 2014). In some of these areas, AVP expression is sexually dimorphic (Rood & De Vries, 2011; Rood *et al.*, 2013; Otero-Garcia *et al.*, 2014). It will be interesting to determine if the GFP is an equally robust reporter in these areas. Substantial evidence further demonstrates that AVP is released by exocytosis fusion not only from neurohypophyseal axon terminals of AVP neurons but also from their dendrites and cell bodies, suggesting neural transmission by the relatively unexplored mechanism of '*dendritic secretion*' (Morris & Pow, 1988; Pow & Morris, 1989; Ludwig, 1998). However, some stimuli induce peptide release from dendrites without increasing the electrical activity of the cell body, and without inducing secretion from axonal terminals (Ludwig & Pittman, 2003; Ludwig & Leng, 2006). Soluble *N*-ethylmaleimide-sensitive factor attachment protein receptor (SNARE) complexes involved in exocytosis in many cells, including exocytosis from synapses and dense-cored vesicle release from neuroendocrine cells (Burgoyne & Morgan, 2003). On the other hands, previous study suggested that '*dendritic secretion*' may use a different molecular mechanism from that described by the SNARE complex theory (Tobin *et al.*, 2012). Thus, the physiological roles of and controls on the novel neural transmission mechanism, '*dendritic secretion*' which AVP (and oxytocin) are released by an

exocytosis not only from the axonal terminals but also from the dendrites and cell bodies of AVP neurons (Morris & Pow, 1988; Pow & Morris, 1989; Ludwig, 1998) remain relatively unexplored. Imaging of GFP signals in AVP-eGFP Tg rats will be able to visualize a response of the dendritic release of AVP against any pharmacological stimulation and elucidate the molecular mechanism of dendritic release.

Copeptin (CP), a 39-aminoacid glycopeptide, is the C-terminal part of the AVP precursor. Activation of the AVP system stimulates CP secretion into the circulation in equimolar amounts to AVP. Thus, CP concentration directly reflects AVP secretion and can be used as a surrogate biomarker because of its stability *in vivo* (Bhandari *et al.*, 2009; Blanchard *et al.*, 2013; Wuttke *et al.*, 2013; Bolignano *et al.*, 2014). Little is known about CP functions *in vivo* (Morgenthaler *et al.*, 2006; Balanescu *et al.*, 2011; Kolonko *et al.*, 2014). In addition, there is lack model animal which can visualize *in vivo* molecular dynamics of CP. Because post-translational modification of the AVP-eGFP fusion gene product results in the formation of a fusion protein: $CP_{1\text{-}14}$-GFP *in vivo*, AVP-eGFP Tg rats will also make it possible to examine the *in vivo* dynamics of CP by analyzing GFP signals.

Oxytocin (OXT) is neurohypophyseal hormone family and one of neurohormones, as well as AVP. OXT is synthesized in neurons of hypothalamus and secreted from the posterior pituitary into the systemic circulation. OXT is classically known to induce labor through increasing uterine tone and promoting uterine contractions (Gimpl & Fahrenholz, 2001). Centrally released OXT is also involved in maternal bonding, sexual behavior, and affiliation (Pedersen *et al.*, 2006; Higashida *et al.*, 2010) and has been implicated in autism, where heightened anxiety levels and deficits in social behavior are common (Grippo *et al.*, 2009). A Tg rat line which

expresses the OXT-monomeric red fluorescent protein (mRFP) fusion gene has been generated (Katoh *et al.*, 2011). In this Tg line, the mRFP is synthesized as a part of the precursor of OXT same as the GFP in the AVP-eGFP Tg rat line. Recently, in OXT-mRFP Tg rats, it is also revealed that the molecular dynamic of RFP is similar to native OXT (Satoh *et al*., in preparation). Thus, OXT-mRFP Tg rats may be a unique model for visualizing the molecular dynamics of OXT *in vivo* and for live imaging and/or electrophysiology of identified OXT neurons without any specific histological labeling. Furthermore, **also in other neurohormones, it may be possible to visualize *in vivo* dynamics by expressing the fluorescent protein as a part of the precursor.**

The conventional *connectome* analysis using exact serial sets of ultrathin sections requires a time-consuming analysis at the ultrastructural level (Hayworth *et al.*, 2014; Henny *et al.*, 2014; Ohno *et al.*, 2015). In Chapter 2, the effective *connectome* analysis using high-voltage electron microscopy (HVEM) tomography has been developed. A novel immune-HVEM tomography applied the special heavy metal staining method, which was originally developed for an enhancement of the membranous contrast for backscattered block-face imaging using scanning electron microscopy (SEM), successfully visualized the three-dimensional (3-D) structure of the itch-mediating neural networks at the synapse level. The *connectome* analysis by HVEM tomography effectively detected numerous itch-mediating synaptic connections in the spinal dorsal horn in thick sections (micrometer order). It is suggested that GRP neurons form more complicated neural networks than expected. Taken together, these results indicated that spinal itch transmission is mediated through the intricate neural networks by the multiple synapses in the rat spinal dorsal horn.

There have been recent advances of imaging techniques for 3-D reconstruction, including the superfine morphological structures observed with focused ion beam-SEM (FIB-SEM) and serial block face (SBF)-SEM (Denk & Horstmann, 2004; Briggman & Denk, 2006; Knott *et al.*, 2008; Namba *et al.*, 2015). These new devices can permit the 3-D reconstruction of a large tissue volume, *i.e.*, the thickness of several hundred micrometers, with visualization of the 3-D subcellular structures or organelles at a fine nanometer scale resolution. Furthermore, an electrically automatic tape-collecting ultra-microtome (ATUM) apparatus has also been developed in recent years (Schalek *et al.*, 2011a; Hayworth *et al.*, 2014). A critical advantage is that pre- and post-embedding immune-EMs are possible in extensive area by continuous ultra-thin sections with the ATUM/SEM. On the other hands, "HVEM tomography" might, at least in part, be superior than such ultra-microtome or beam-milling techniques in quick and repeated examinations. Moreover, HVEM tomography may also have some advantages, compared with the ATUM, and be more effective in the volume EM analysis with less failure after identification of an observation area by light microscopy. Compared with these 3-D SEM methods, "HVEM tomography" has the following characteristics and advantages: 1) quick observation of a large area, 2) less thermal denaturation, and also 3) no tissue destruction. While the SEM-image acquisition time is limited by the scanning speed, "HVEM tomography" (semi-thin sections) only needs the time required to collect a whole tilt series of the specimen. Thus, HVEM methodology is more useful and effective because it correlates well between light and electron microscopes. On the other hand, a major advantage of other 3-D scanning electron microscopies is that it is possible to acquire an exact series of the high contrast images, which is the same as a set of transmission electron microscopy images obtained from a number of serial

ultra-thin sections. Thus, there are many advantages in both the new *connectome* techniques and HVEM tomography, and each technique has specific advantages. Moreover, the HVEM methodology used in this study is simple and can be applied in multiple ways. This is an important contribution to ultrastructural investigations of the central nervous system in the present post-genomic age.

In conclusion, in this study, it is established a model which can visualize molecular dynamics such as intracellular transport and exocytosis underlying neuroendocrine dynamics. In addition, present study revealed part of molecular dynamics related to post-translational processing. Moreover, efficient *connectome* analysis was developed, and it is revealed a part of peptidergic neural network in itch sensory transmission by using this useful HVEM methodology. These advanced methods will be applicable not only to AVP and GRP but also to other neurohormones. The combination of an imaging model and a useful HVEM methodology will make inclusively visualization possible the intracellular molecular dynamics and neural network of neurohormones. This combinated methods would be able to elucidate the peptidergic control circuit for neuroendocrine dynamics basis of molecular dynamics and neural network.

Acknowledgements

I am grateful to my supervisor Associate Prof. Hirotaka Sakamoto for his valuable comments and disscussions through this work. I also thank Profs. Sumio Takahashi and Tatsuya Sakamoto for their valuable comments and encouragement on this work. I also thank Drs. Naoaki Tsutsui, Yasuhisa Kobayashi, Mayuko Hamada, Keiko Takanami, and Takumi Oti for their valuable comments and encouragement on this work. I would like to thank Profs. John F. Morris, Mitsuhiro Kawata, Yoichi Ueta, and Kazuyoshi Murata for valuable comments and suggestions on this work. The discussion and cooperation with all colleagues have contributed substantially to this work. I would like to acknowledge the Japan Society for the Promotion of Science (JSPS) for supporting me a Reseach Fellowship for Young Scientists.

References

Albers, H.E. (2014) Species, sex and individual differences in the vasotocin/vasopressin system: Relationship to neurochemical signaling in the social behavior neural network. *Front Neuroendocrinol*.

Axelrod, D. (1981) Cell-substrate contacts illuminated by total internal reflection fluorescence. *J Cell Biol*, **89**, 141-145.

Balanescu, S., Kopp, P., Gaskill, M.B., Morgenthaler, N.G., Schindler, C. & Rutishauser, J. (2011) Correlation of plasma copeptin and vasopressin concentrations in hypo-, iso-, and hyperosmolar States. *J Clin Endocrinol Metab*, **96**, 1046-1052.

Belichenko, P.V. & Dahlstrom, A. (1995) Studies on the 3-dimensional architecture of dendritic spines and varicosities in human cortex by confocal laser scanning microscopy and Lucifer yellow microinjections. *J Neurosci Methods*, **57**, 55-61.

Bhandari, S.S., Loke, I., Davies, J.E., Squire, I.B., Struck, J. & Ng, L.L. (2009) Gender and renal function influence plasma levels of copeptin in healthy individuals. *Clin Sci (Lond)*, **116**, 257-263.

Birnbaumer, M., Antaramian, A., Themmen, A.P. & Gilbert, S. (1992a) Desensitization of the human V2 vasopressin receptor. Homologous effects in the absence of heterologous desensitization. *J Biol Chem*, **267**, 11783-11788.

Birnbaumer, M., Seibold, A., Gilbert, S., Ishido, M., Barberis, C., Antaramian, A., Brabet, P. & Rosenthal, W. (1992b) Molecular cloning of the receptor for human antidiuretic hormone. *Nature*, **357**, 333-335.

Blanchard, A., Steichen, O., De Mota, N., Curis, E., Gauci, C., Frank, M., Wuerzner, G., Kamenicky, P., Passeron, A., Azizi, M. & Llorens-Cortes, C. (2013) An abnormal apelin/vasopressin balance may contribute to water retention in patients with the syndrome of inappropriate antidiuretic hormone (SIADH) and heart failure. *J Clin Endocrinol Metab*, **98**, 2084-2089.

Boertien, W.E., Meijer, E., Zittema, D., van Dijk, M.A., Rabelink, T.J., Breuning, M.H.,

Struck, J., Bakker, S.J., Peters, D.J., de Jong, P.E. & Gansevoort, R.T. (2012) Copeptin, a surrogate marker for vasopressin, is associated with kidney function decline in subjects with autosomal dominant polycystic kidney disease. *Nephrol Dial Transplant*, **27**, 4131-4137.

Bolignano, D., Cabassi, A., Fiaccadori, E., Ghigo, E., Pasquali, R., Peracino, A., Peri, A., Plebani, M., Santoro, A., Settanni, F. & Zoccali, C. (2014) Copeptin (CTproAVP), a new tool for understanding the role of vasopressin in pathophysiology. *Clin Chem Lab Med*.

Briggman, K.L. & Denk, W. (2006) Towards neural circuit reconstruction with volume electron microscopy techniques. *Curr Opin Neurobiol*, **16**, 562-570.

Buma, P., Roubos, E.W. & Buijs, R.M. (1984) Ultrastructural demonstration of exocytosis of neural, neuroendocrine and endocrine secretions with an in vitro tannic acid (TARI-) method. *Histochemistry*, **80**, 247-256.

Burbach, J.P. (2010) Neuropeptides from concept to online database http://www.neuropeptides.nl/. *Eur J Pharmacol*, **626**, 27-48.

Burckhardt, M.A., Wellmann, M., Fouzas, S., Lapaire, O., Burkhardt, T., Benzing, J., Buhrer, C., Szinnai, G. & Wellmann, S. (2014) Sexual Disparity of Copeptin in Healthy Newborn Infants. *J Clin Endocrinol Metab*, **99**, E1750-E1753.

Burgoyne, R.D. & Morgan, A. (2003) Secretory granule exocytosis. *Physiol Rev*, **83**, 581-632.

Castel, M., Morris, J. & Belenky, M. (1996) Non-synaptic and dendritic exocytosis from dense-cored vesicles in the suprachiasmatic nucleus. *Neuroreport*, **7**, 543-547.

Castel, M., Morris, J.F., Whitnall, M.H. & Sivan, N. (1986) Improved visualization of the immunoreactive hypothalamo-neurohypophysial system by use of immuno-gold techniques. *Cell Tissue Res*, **243**, 193-204.

Cazalis, M., Dayanithi, G. & Nordmann, J.J. (1985) The role of patterned burst and interburst interval on the excitation-coupling mechanism in the isolated rat neural lobe.

J Physiol, **369**, 45-60.

Davies, J., Waller, S., Zeng, Q., Wells, S. & Murphy, D. (2003) Further delineation of the sequences required for the expression and physiological regulation of the vasopressin gene in transgenic rat hypothalamic magnocellular neurones. *J Neuroendocrinol*, **15**, 42-50.

Deerinck, T., Bushong, E., Thor, A. & Ellisman, M. (2010) NCMIR methods for 3D EM: a new protocol for preparation of biological specimens for serial block face scanning electron microscopy., San Diego, CA.

Denk, W. & Horstmann, H. (2004) Serial block-face scanning electron microscopy to reconstruct three-dimensional tissue nanostructure. *PLoS Biol*, **2**, e329.

Denk, W. & Svoboda, K. (1997) Photon upmanship: why multiphoton imaging is more than a gimmick. *Neuron*, **18**, 351-357.

Fleming, M.S., Ramos, D., Han, S.B., Zhao, J., Son, Y.J. & Luo, W. (2012) The majority of dorsal spinal cord gastrin releasing peptide is synthesized locally whereas neuromedin B is highly expressed in pain- and itch-sensing somatosensory neurons. *Mol Pain*, **8**, 52.

Fujihara, H., Ueta, Y., Suzuki, H., Katoh, A., Ohbuchi, T., Otsubo, H., Dayanithi, G. & Murphy, D. (2009) Robust up-regulation of nuclear red fluorescent-tagged fos marks neuronal activation in green fluorescent vasopressin neurons after osmotic stimulation in a double-transgenic rat. *Endocrinology*, **150**, 5633-5638.

Fujio, T., Fujihara, H., Shibata, M., Yamada, S., Onaka, T., Tanaka, K., Morita, H., Dayanithi, G., Kawata, M., Murphy, D. & Ueta, Y. (2006) Exaggerated response of arginine vasopressin-enhanced green fluorescent protein fusion gene to salt loading without disturbance of body fluid homeostasis in rats. *J Neuroendocrinol*, **18**, 776-785.

Gimpl, G. & Fahrenholz, F. (2001) The oxytocin receptor system: structure, function, and regulation. *Physiol Rev*, **81**, 629-683.

Grippo, A.J., Trahanas, D.M., Zimmerman, R.R., 2nd, Porges, S.W. & Carter, C.S.

(2009) Oxytocin protects against negative behavioral and autonomic consequences of long-term social isolation. *Psychoneuroendocrinology*, **34**, 1542-1553.

Hama, K. & Kosaka, T. (1981) Neurobiological Applications of High-Voltage Electron-Microscopy. *Trends Neurosci*, **4**, 193-196.

Hashimoto, M., Sakamoto, S. & Ikeda, M. (2015) Clinical features of delusional jealousy in elderly patients with dementia. *J Clin Psychiatry*, **76**, 691-695.

Hayworth, K.J., Morgan, J.L., Schalek, R., Berger, D.R., Hildebrand, D.G. & Lichtman, J.W. (2014) Imaging ATUM ultrathin section libraries with WaferMapper: a multi-scale approach to EM reconstruction of neural circuits. *Front Neural Circuits*, **8**, 68.

Henny, P., Brown, M.T., Micklem, B.R., Magill, P.J. & Bolam, J.P. (2014) Stereological and ultrastructural quantification of the afferent synaptome of individual neurons. *Brain Struct Funct*, **219**, 631-640.

Higashida, H., Lopatina, O., Yoshihara, T., Pichugina, Y.A., Soumarokov, A.A., Munesue, T., Minabe, Y., Kikuchi, M., Ono, Y., Korshunova, N. & Salmina, A.B. (2010) Oxytocin signal and social behaviour: comparison among adult and infant oxytocin, oxytocin receptor and CD38 gene knockout mice. *J Neuroendocrinol*, **22**, 373-379.

Inami, H., Shishikura, J., Yasunaga, T., Ohno, K., Yamashita, H., Kato, K. & Sakamoto, S. (2015) Synthesis, structure-activity relationships, and anticonvulsant activities of 2-amino-4H-pyrido[3,2-e][1,3]thiazin-4-one derivatives as orally active AMPA receptor antagonists. *Bioorg Med Chem*, **23**, 1788-1799.

Iwanaga, M., Ohno, M., Katoh, A., Ohbuchi, T., Ishikura, T., Fujihara, H., Nomura, M., Hachisuka, K. & Ueta, Y. (2011) Upregulation of arginine vasopressin synthesis in the rat hypothalamus after kainic acid-induced seizures. *Brain Res*, **1424**, 1-8.

Katoh, A., Fujihara, H., Ohbuchi, T., Onaka, T., Hashimoto, T., Kawata, M., Suzuki, H. & Ueta, Y. (2011) Highly visible expression of an oxytocin-monomeric red fluorescent protein 1 fusion gene in the hypothalamus and posterior pituitary of transgenic rats. *Endocrinology*, **152**, 2768-2774.

Kawasaki, M., Yamaguchi, K., Saito, J., Ozaki, Y., Mera, T., Hashimoto, H., Fujihara, H., Okimoto, N., Ohnishi, H., Nakamura, T. & Ueta, Y. (2005) Expression of immediate early genes and vasopressin heteronuclear RNA in the paraventricular and supraoptic nuclei of rats after acute osmotic stimulus. *J Neuroendocrinol*, **17**, 227-237.

Kishimoto, T., Kimura, R., Liu, T.T., Nemoto, T., Takahashi, N. & Kasai, H. (2006) Vacuolar sequential exocytosis of large dense-core vesicles in adrenal medulla. *EMBO J*, **25**, 673-682.

Knott, G., Marchman, H., Wall, D. & Lich, B. (2008) Serial section scanning electron microscopy of adult brain tissue using focused ion beam milling. *J Neurosci*, **28**, 2959-2964.

Kolonko, A., Chudek, J., Kujawa-Szewieczek, A., Czerwienska, B. & Wiecek, A. (2014) Serum copeptin level predicts a rapid decrease of overhydration after kidney transplantation. *Clin Chem Lab Med*, **52**, 1297-1303.

Koshimizu, T.A., Nakamura, K., Egashira, N., Hiroyama, M., Nonoguchi, H. & Tanoue, A. (2012) Vasopressin V1a and V1b receptors: from molecules to physiological systems. *Physiol Rev*, **92**, 1813-1864.

Kremer, J.R., Mastronarde, D.N. & McIntosh, J.R. (1996) Computer visualization of three-dimensional image data using IMOD. *J Struct Biol*, **116**, 71-76.

Land, H., Schutz, G., Schmale, H. & Richter, D. (1982) Nucleotide sequence of cloned cDNA encoding bovine arginine vasopressin-neurophysin II precursor. *Nature*, **295**, 299-303.

Lolait, S.J., O'Carroll, A.M., McBride, O.W., Konig, M., Morel, A. & Brownstein, M.J. (1992) Cloning and characterization of a vasopressin V2 receptor and possible link to nephrogenic diabetes insipidus. *Nature*, **357**, 336-339.

Ludwig, M. (1998) Dendritic release of vasopressin and oxytocin. *J Neuroendocrinol*, **10**, 881-895.

Ludwig, M. & Leng, G. (2006) Dendritic peptide release and peptide-dependent

behaviours. *Nat Rev Neurosci*, **7**, 126-136.

Ludwig, M. & Pittman, Q.J. (2003) Talking back: dendritic neurotransmitter release. *Trends Neurosci*, **26**, 255-261.

Ludwig, M., Sabatier, N., Bull, P.M., Landgraf, R., Dayanithi, G. & Leng, G. (2002) Intracellular calcium stores regulate activity-dependent neuropeptide release from dendrites. *Nature*, **418**, 85-89.

Maruyama, T., Ohbuchi, T., Fujihara, H., Shibata, M., Mori, K., Murphy, D., Dayanithi, G. & Ueta, Y. (2010) Diurnal changes of arginine vasopressin-enhanced green fluorescent protein fusion transgene expression in the rat suprachiasmatic nucleus. *Peptides*, **31**, 2089-2093.

Meijer, E., de Jong, P.E. & Gansevoort, R.T. (2010) Vasopressin and microalbuminuria: is it vasopressin per se or is it salt intake? *Kidney Int*, **77**, 832-833.

Meyer-Lindenberg, A., Domes, G., Kirsch, P. & Heinrichs, M. (2011) Oxytocin and vasopressin in the human brain: social neuropeptides for translational medicine. *Nat Rev Neurosci*, **12**, 524-538.

Miyawaki, A. (2003) Fluorescence imaging of physiological activity in complex systems using GFP-based probes. *Curr Opin Neurobiol*, **13**, 591-596.

Morgenthaler, N.G., Struck, J., Alonso, C. & Bergmann, A. (2006) Assay for the measurement of copeptin, a stable peptide derived from the precursor of vasopressin. *Clin Chem*, **52**, 112-119.

Moritoh, S., Sato, K., Okada, Y. & Koizumi, A. (2011) Endogenous arginine vasopressin-positive retinal cells in arginine vasopressin-eGFP transgenic rats identified by immunohistochemistry and reverse transcriptase-polymerase chain reaction. *Mol Vis*, **17**, 3254-3261.

Morris, J.F. & Pow, D.V. (1988) Capturing and quantifying the exocytotic event. *J Exp Biol*, **139**, 81-103.

Namba, K., Goto, H., Kaburaki, T., Kitaichi, N., Mizuki, N., Asukata, Y., Fujino, Y., Meguro, A., Sakamoto, S., Shibuya, E., Yokoi, K. & Ohno, S. (2015) A Major Review: Current Aspects of Ocular Behcet's Disease in Japan. *Ocul Immunol Inflamm*, **23 Suppl 1**, S1-23.

Nishi, M. & Kawata, M. (2006) Brain corticosteroid receptor dynamics and trafficking: Implications from live cell imaging. *Neuroscientist*, **12**, 119-133.

Ohbuchi, T., Yokoyama, T., Saito, T., Hashimoto, H., Suzuki, H., Otsubo, H., Fujihara, H. & Ueta, Y. (2009) Brain-derived neurotrophic factor inhibits spontaneous inhibitory postsynaptic currents in the rat supraoptic nucleus. *Brain Res*, **1258**, 34-42.

Ohbuchi, T., Yokoyama, T., Saito, T., Suzuki, H., Fujihara, H., Katoh, A., Otsubo, H., Ishikura, T. & Ueta, Y. (2010) Modulators of BK and SK channels alter electrical activity in vitro in single vasopressin neurons isolated from the rat supraoptic nucleus. *Neurosci Lett*, **484**, 26-29.

Ohkubo, J., Ohbuchi, T., Yoshimura, M., Maruyama, T., Ishikura, T., Matsuura, T., Suzuki, H. & Ueta, Y. (2014) Electrophysiological effects of kainic Acid on vasopressin-enhanced green fluorescent protein and oxytocin-monomeric red fluorescent protein 1 neurones isolated from the supraoptic nucleus in transgenic rats. *J Neuroendocrinol*, **26**, 43-51.

Ohno, N., Katoh, M., Saitoh, Y., Saitoh, S. & Ohno, S. (2015) Three-dimensional volume imaging with electron microscopy toward connectome. *Microscopy (Oxf)*, **64**, 17-26.

Okabe, S. (2013) Fluorescence imaging of synapse formation and remodeling. *Microscopy (Oxf)*, **62**, 51-62.

Otero-Garcia, M., Martin-Sanchez, A., Fortes-Marco, L., Martinez-Ricos, J., Agustin-Pavon, C., Lanuza, E. & Martinez-Garcia, F. (2014) Extending the socio-sexual brain: arginine-vasopressin immunoreactive circuits in the telencephalon of mice. *Brain Struct Funct*, **219**, 1055-1081.

Oti, T., Satoh, K., Saito, K., Murata, K., Kawata, M., Sakamoto, T. & Sakamoto, H.

(2012) Three-dimensional evaluation of the spinal local neural network revealed by the high-voltage electron microscopy: a double immunohistochemical study. *Histochem Cell Biol*, **138**, 693-697.

Pedersen, C.A., Vadlamudi, S.V., Boccia, M.L. & Amico, J.A. (2006) Maternal behavior deficits in nulliparous oxytocin knockout mice. *Genes Brain Behav*, **5**, 274-281.

Pettersen, E.F., Goddard, T.D., Huang, C.C., Couch, G.S., Greenblatt, D.M., Meng, E.C. & Ferrin, T.E. (2004) UCSF Chimera--a visualization system for exploratory research and analysis. *J Comput Chem*, **25**, 1605-1612.

Pow, D.V. & Morris, J.F. (1989) Dendrites of hypothalamic magnocellular neurons release neurohypophysial peptides by exocytosis. *Neuroscience*, **32**, 435-439.

Rood, B.D. & De Vries, G.J. (2011) Vasopressin innervation of the mouse (Mus musculus) brain and spinal cord. *J Comp Neurol*, **519**, 2434-2474.

Rood, B.D., Stott, R.T., You, S., Smith, C.J., Woodbury, M.E. & De Vries, G.J. (2013) Site of origin of and sex differences in the vasopressin innervation of the mouse (Mus musculus) brain. *J Comp Neurol*, **521**, 2321-2358.

Sakamoto, H., Arii, T. & Kawata, M. (2010) High-voltage electron microscopy reveals direct synaptic inputs from a spinal gastrin-releasing peptide system to neurons of the spinal nucleus of bulbocavernosus. *Endocrinology*, **151**, 417-421.

Sakamoto, H. & Kawata, M. (2012) Ultrahigh voltage electron microscopy links neuroanatomy and neuroscience/neuroendocrinology. *Anatomy research international*, **2012**, 948704.

Sakamoto, H., Matsuda, K., Hosokawa, K., Nishi, M., Morris, J.F., Prossnitz, E.R. & Kawata, M. (2007) Expression of G protein-coupled receptor-30, a G protein-coupled membrane estrogen receptor, in oxytocin neurons of the rat paraventricular and supraoptic nuclei. *Endocrinology*, **148**, 5842-5850.

Sato, M., Kitaguchi, T., Numano, R., Ikematsu, K., Kakeyama, M., Murata, M., Sato, K. & Tsuboi, T. (2012) The small GTPase Cdc42 modulates the number of

exocytosis-competent dense-core vesicles in PC12 cells. *Biochem Biophys Res Commun*, **420**, 417-421.

Satoh, K., Takanami, K., Murata, K., Kawata, M., Sakamoto, T. & Sakamoto, H. (2015) Three-dimensional visualization of multiple synapses in thick sections using high-voltage electron microscopy in the rat spinal cord. *Data Brief*, **4**, 566-570.

Schalek, R., Kasthuri, N., Hayworth, K., Berger, D., Tapia, J., Morgan, J., Turaga, S., Fagerholm, E., Seung, H. & Lichtman, J. (2011a) Development of high-throughput, high-resolution 3D reconstruction of large-volume biological tissue using automated tape collection ultramicrotomy and scanning electron microscopy. *Microsc Microanal*, **17**, 966-967.

Schalek, R., Kasthuri, N., Hayworth, K., Berger, D., Tapia, J., Morgan, J., Turaga, S., Fagerholm, E., Seung, H. & Lichtman, J. (2011b) Development of High-Throughput, High-Resolution 3D Reconstruction of Large-Volume Biological Tissue Using Automated Tape Collection Ultramicrotomy and Scanning Electron Microscopy. *Microscopy and Microanalysis*, **17**, 966-967.

Schlapbach, L.J., Frey, S., Bigler, S., Manh-Nhi, C., Aebi, C., Nelle, M. & Nuoffer, J.M. (2011) Copeptin concentration in cord blood in infants with early-onset sepsis, chorioamnionitis and perinatal asphyxia. *BMC Pediatr*, **11**, 38.

Sherman, T.G., McKelvy, J.F. & Watson, S.J. (1986) Vasopressin mRNA regulation in individual hypothalamic nuclei: a northern and in situ hybridization analysis. *J Neurosci*, **6**, 1685-1694.

Shibata, M., Fujihara, H., Suzuki, H., Ozawa, H., Kawata, M., Dayanithi, G., Murphy, D. & Ueta, Y. (2007) Physiological studies of stress responses in the hypothalamus of vasopressin-enhanced green fluorescent protein transgenic rat. *J Neuroendocrinol*, **19**, 285-292.

Sun, Y.G. & Chen, Z.F. (2007) A gastrin-releasing peptide receptor mediates the itch sensation in the spinal cord. *Nature*, **448**, 700-703.

Sun, Y.G., Zhao, Z.Q., Meng, X.L., Yin, J., Liu, X.Y. & Chen, Z.F. (2009) Cellular basis

of itch sensation. *Science*, **325**, 1531-1534.

Suzuki, H., Kawasaki, M., Ohnishi, H., Otsubo, H., Ohbuchi, T., Katoh, A., Hashimoto, H., Yokoyama, T., Fujihara, H., Dayanithi, G., Murphy, D., Nakamura, T. & Ueta, Y. (2009a) Exaggerated response of a vasopressin-enhanced green fluorescent protein transgene to nociceptive stimulation in the rat. *J Neurosci*, **29**, 13182-13189.

Suzuki, H., Onaka, T., Kasai, M., Kawasaki, M., Ohnishi, H., Otsubo, H., Saito, T., Hashimoto, H., Yokoyama, T., Fujihara, H., Dayanithi, G., Murphy, D., Nakamura, T. & Ueta, Y. (2009b) Response of arginine vasopressin-enhanced green fluorescent protein fusion gene in the hypothalamus of adjuvant-induced arthritic rats. *J Neuroendocrinol*, **21**, 183-190.

Szinnai, G., Morgenthaler, N.G., Berneis, K., Struck, J., Muller, B., Keller, U. & Christ-Crain, M. (2007) Changes in plasma copeptin, the c-terminal portion of arginine vasopressin during water deprivation and excess in healthy subjects. *J Clin Endocrinol Metab*, **92**, 3973-3978.

Takahashi, N., Kishimoto, T., Nemoto, T., Kadowaki, T. & Kasai, H. (2002) Fusion pore dynamics and insulin granule exocytosis in the pancreatic islet. *Science*, **297**, 1349-1352.

Takanami, K. & Sakamoto, H. (2014) The Gastrin-Releasing Peptide Receptor (GRPR) in the Spinal Cord as a Novel Pharmacological Target. *Curr Neuropharmacol*, **12**, 434-443.

Takanami, K., Sakamoto, H., Matsuda, K.I., Satoh, K., Tanida, T., Yamada, S., Inoue, K., Oti, T., Sakamoto, T. & Kawata, M. (2014) Distribution of gastrin-releasing peptide in the rat trigeminal and spinal somatosensory systems. *J Comp Neurol*, **522**, 1858-1873.

Tobin, V., Schwab, Y., Lelos, N., Onaka, T., Pittman, Q.J. & Ludwig, M. (2012) Expression of exocytosis proteins in rat supraoptic nucleus neurones. *J Neuroendocrinol*, **24**, 629-641.

Todoroki, M., Ueta, Y., Fujihara, H., Otsubo, H., Shibata, M., Hashimoto, H., Kobayashi, M., Sakamoto, H., Kawata, M., Dayanithi, G., Murphy, D., Hiro, H., Takahashi, K. &

Nagata, S. (2010) Induction of the arginine vasopressin-enhanced green fluorescent protein fusion transgene in the rat locus coeruleus. *Stress*, **13**, 281-291.

Tsuboi, T. & Fukuda, M. (2005) The C2B domain of rabphilin directly interacts with SNAP-25 and regulates the docking step of dense core vesicle exocytosis in PC12 cells. *J Biol Chem*, **280**, 39253-39259.

Tsuboi, T. & Fukuda, M. (2006a) Rab3A and Rab27A cooperatively regulate the docking step of dense-core vesicle exocytosis in PC12 cells. *J Cell Sci*, **119**, 2196-2203.

Tsuboi, T. & Fukuda, M. (2006b) The Slp4-a linker domain controls exocytosis through interaction with Munc18-1.syntaxin-1a complex. *Mol Biol Cell*, **17**, 2101-2112.

Tsuboi, T., Kanno, E. & Fukuda, M. (2007) The polybasic sequence in the C2B domain of rabphilin is required for the vesicle docking step in PC12 cells. *J Neurochem*, **100**, 770-779.

Ueta, Y., Fujihara, H., Serino, R., Dayanithi, G., Ozawa, H., Matsuda, K., Kawata, M., Yamada, J., Ueno, S., Fukuda, A. & Murphy, D. (2005) Transgenic expression of enhanced green fluorescent protein enables direct visualization for physiological studies of vasopressin neurons and isolated nerve terminals of the rat. *Endocrinology*, **146**, 406-413.

Viero, C., Shibuya, I., Kitamura, N., Verkhratsky, A., Fujihara, H., Katoh, A., Ueta, Y., Zingg, H.H., Chvatal, A., Sykova, E. & Dayanithi, G. (2010) REVIEW: Oxytocin: Crossing the bridge between basic science and pharmacotherapy. *CNS Neurosci Ther*, **16**, e138-156.

Wang, H., Ward, A.R. & Morris, J.F. (1995) Oestradiol acutely stimulates exocytosis of oxytocin and vasopressin from dendrites and somata of hypothalamic magnocellular neurons. *Neuroscience*, **68**, 1179-1188.

Wotjak, C.T., Ganster, J., Kohl, G., Holsboer, F., Landgraf, R. & Engelmann, M. (1998) Dissociated central and peripheral release of vasopressin, but not oxytocin, in response to repeated swim stress: new insights into the secretory capacities of peptidergic neurons. *Neuroscience*, **85**, 1209-1222.

Wuttke, A., Dixit, K.C., Szinnai, G., Werth, S.C., Haagen, U., Christ-Crain, M., Morgenthaler, N. & Brabant, G. (2013) Copeptin as a marker for arginine-vasopressin/antidiuretic hormone secretion in the diagnosis of paraneoplastic syndrome of inappropriate ADH secretion. *Endocrine*, **44**, 744-749.

Yao, S.T., Antunes, V.R., Bradley, P.M., Kasparov, S., Ueta, Y., Paton, J.F. & Murphy, D. (2011) Temporal profile of arginine vasopressin release from the neurohypophysis in response to hypertonic saline and hypotension measured using a fluorescent fusion protein. *J Neurosci Methods*, **201**, 191-195.